

Learning to Translate Noise for Robust Image Denoising

Inju Ha^{*1} Donghun Ryou^{*2} Seonguk Seo³ Bohyung Han^{1,2}
¹ECE & ²IPAI, Seoul National University ³Meta
{hij1112, dhryou, bhhan}@snu.ac.kr seonguk@meta.com
<https://hij1112.github.io/learning-to-translate-noise/>

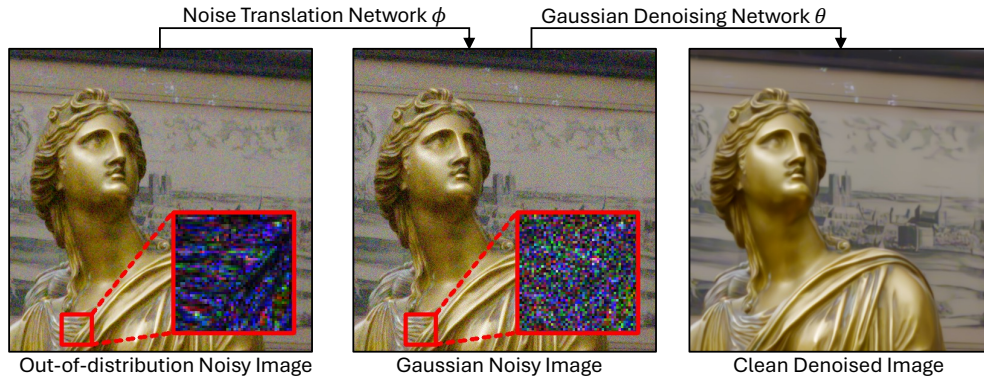


Figure 1. Our noise translation network (NTN) first transforms arbitrary real-world noise into Gaussian noise without signal correlation. The translated noise can then be effectively removed using any existing Gaussian denoiser. The shown noisy image is from the NIND dataset [3], captured at ISO 6400. The figure is best viewed by zooming in.

Abstract

Image denoising techniques based on deep learning often struggle with poor generalization performance to out-of-distribution real-world noise. To tackle this challenge, we propose a novel noise translation framework that performs denoising on an image with translated noise rather than directly denoising an original noisy image. Specifically, our approach translates unknown real-world noise into Gaussian noise, which is spatially uncorrelated and independent of image content, through our noise translation network. The translated noisy images are then processed by an image denoising network pretrained to effectively remove Gaussian noise, enabling robust and consistent denoising performance. We also design well-motivated loss functions and architectures for the noise translation network by leveraging the mathematical properties of Gaussian noise. Experimental results show that the proposed approach substantially improves robustness and generalizability, outperforming state-of-the-art methods across diverse benchmarks.

1. Introduction

Image denoising aims to restore the pure signal from noisy images and serves as a critical preprocessing step to im-

prove the visual quality of input images, extending the applicability to various downstream tasks. Recent advances in deep learning facilitate significant performance improvement of image denoising models [6, 10, 36, 42–47]. A common assumption in early approaches was that camera noise could be modeled as a Gaussian distribution [28, 46, 47], which simplified the process of generating noisy-clean image pairs by adding synthetic Gaussian noise. This allowed for the construction of large datasets that could be used to train denoising models in a supervised manner, playing a crucial role in advancing image denoising models.

While denoising models trained on synthetic datasets perform well in controlled environments, they struggle to generalize to real-world scenarios due to the fundamental differences between synthetic and real noise distributions [10]. In response, researchers collected clean-noisy image pairs from real images [1, 38, 40] to address realistic noises, but denoising models still tend to overfit to the specific noise-signal correlations present in the training data. Capturing the full spectrum of real-world noise distributions to prevent overfitting is impractical and even unrealistic.

To address this challenge, we propose a novel noise translation framework for image denoising to better generalize to diverse real-world noise using a limited training dataset. The intuition behind our framework is as follows.

^{*}indicates equal contribution.

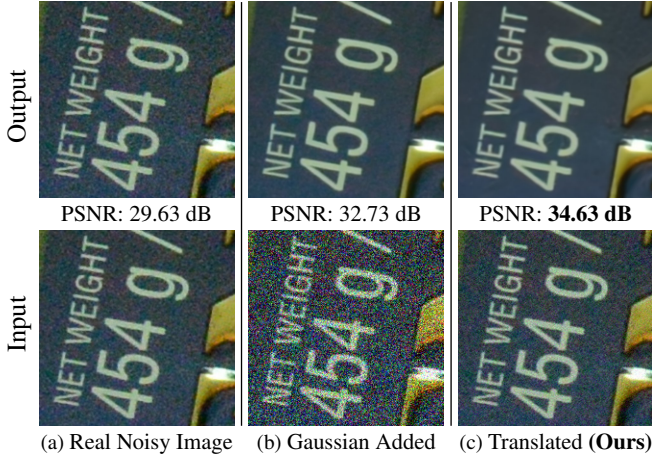


Figure 2. Denoising results of Gaussian-trained Restormer [43]. From left to right: (1) real noisy image and its denoised output, (2) noisy image with added Gaussian noise and its denoised output, (3) noise-translated image with our framework and its corresponding denoised output, achieving superior quality.

While existing denoising algorithms trained on images with Gaussian noise exhibit limited performance when applied to real-world noisy images, we observed that adding Gaussian noise to these noisy images significantly improves their effectiveness in denoising, as shown in Figure 2. This observation motivated us to explore the idea that, instead of directly denoising unseen real noise, first translating it into known Gaussian noise and then applying denoising could improve the model’s ability to generalize across unseen out-of-distribution (OOD) noise. To this end, we introduce the lightweight *Noise Translation Network*, which, prior to the denoising process, utilizes Gaussian injection blocks to transform arbitrary complex noise into Gaussian noise that is spatially uncorrelated and independent of an input image. The translated images are then processed by the pretrained denoising networks specialized for Gaussian noise, resulting in the clean denoised images. Once trained, our noise translation network can be seamlessly paired with any denoising network pretrained on Gaussian noise. Our experimental results and analysis validate that the proposed framework outperforms existing denoising approaches by huge margins on various benchmarks.

Our key contributions are summarized as follows:

- We propose a novel noise translation network for robust image denoising that converts unseen complex noise in an input image into Gaussian noise. Our lightweight noise translation network can seamlessly integrate with any Gaussian-pretrained denoising networks.
- We employ well-motivated loss functions and architecture for the noise translation network. Our translation network transforms the noise distribution of the input image into a Gaussian distribution both implicitly and explicitly by leveraging key mathematical properties.

- We demonstrate the efficacy of our approach through extensive experiments on image denoising benchmarks with diverse noise distributions, achieving significant improvements in terms of robustness and generalization ability.

2. Related Works

Image denoising In recent years, deep learning has led to significant progress in image restoration [6, 7, 13, 35, 43], achieving impressive results by leveraging paired noisy and clean images for training. DnCNN [46] pioneered the use of CNNs for image denoising, which paved the way for further advancements involving residual learning [9, 23, 48], attention mechanisms [22, 48], and transformer models [43, 45]. Despite its success, acquiring the noisy-clean pairs required for supervised training remains a significant challenge. To address this, self-supervised approaches [2, 18, 20, 21, 32] have emerged to train networks using only noisy images, but these models typically perform considerably worse than their supervised counterparts. Additionally, zero-shot approaches [11, 27, 33] have been proposed for image denoising even without a training dataset, but they require substantial computational cost at inference, making them impractical for real-time applications. While previous methods either rely heavily on supervised datasets or bypass them with performance trade-offs, we show that robust generalization is achievable even under limited supervision. This makes it suitable for real-world deployment, where collecting large-scale clean references remains a major bottleneck.

Generalization for denoising Generalization is a critical challenge in image denoising, as the performance of denoising models often degrades when encountering noise characteristics that were not seen during training. To handle unseen noise type or levels, DnCNN [46] employed blind Gaussian training to adapt to various noise levels, while Mohan *et al.* [30] designed a bias-free network to prevent overfitting to noise levels in the training set. Recent works employed masking-based learning [5] or leveraged the pretrained CLIP encoder [8] to prevent overfitting by encouraging the model to understand global context rather than relying on local patterns. In addition, IDF [15] introduced an iterative dynamic filtering to better generalize to unseen noise. While these approaches enhance robustness to unseen noise, they often struggle to produce high-quality images, particularly in complex real-world scenarios.

To handle real-world noise, prior work has focused on building training datasets that reflect realistic noise distributions. This includes collecting real clean-noisy image pairs [1, 38, 40], simulating realistic noise via data augmentation [4, 12, 41], or leveraging adversarial training [34, 39]. However, these approaches are inherently limited by the noise distributions seen during training and often fail to generalize to out-of-distribution (OOD) noise. Alternatively,

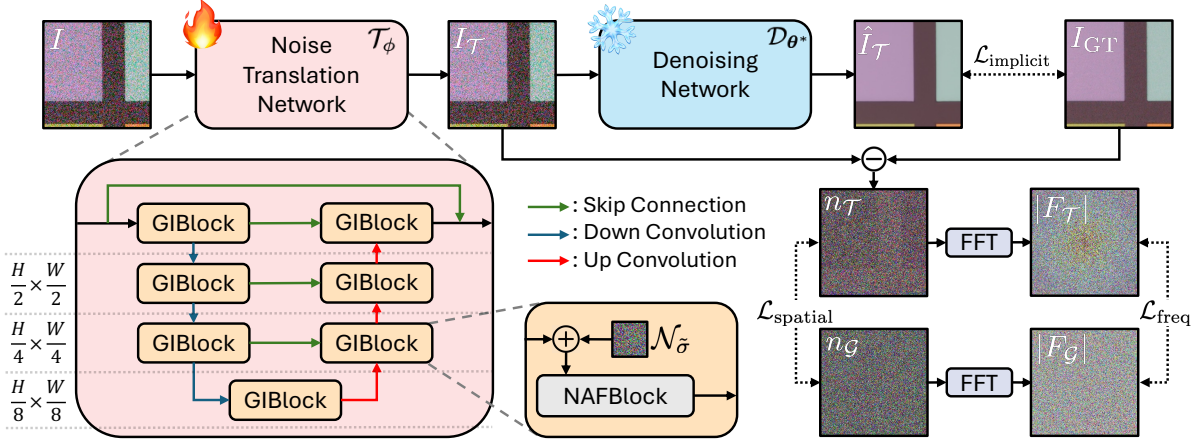


Figure 3. Illustration of our training framework for the noise translation network.

noise transformation methods such as the Anscombe transform [26] and pixel-shuffle down-sampling [50] aim to simplify denoising by converting complex noise into Gaussian-like noise. However, their reliance on fixed transformations limits their adaptability to diverse noise types. More recently, LAN [14] addressed unseen noise through test-time optimization of pixel-wise offsets. While effective, its per-pixel updates hinder scalability to images larger than 256×256 . In contrast, our approach removes the need for test-time training and enables efficient, scalable denoising under a wide range of noise conditions.

3. Image Denoising through Noise Translation

This section presents our robust image denoising framework with a novel noise translation process, designed to handle diverse real-world noise. Our framework first transforms a noisy image I into an image with Gaussian noise $I_{\mathcal{T}}$, which is then fed into the denoising network to produce the final denoised output $\hat{I}_{\mathcal{T}}$. The whole process is given by

$$\hat{I}_{\mathcal{T}} = \mathcal{D}(I_{\mathcal{T}}; \theta) = \mathcal{D}(\mathcal{T}(I; \phi); \theta), \quad (1)$$

where $\mathcal{T}(\cdot; \phi)$ denotes the noise translation network parametrized by ϕ , and $\mathcal{D}(\cdot; \theta)$ indicates the denoising network with parameters θ . Note that $\mathcal{D}(\cdot; \theta)$ is specialized in handling Gaussian noise in our framework. We next discuss how to train the denoising network $\mathcal{D}(\cdot; \theta)$ and noise translation network $\mathcal{T}(\cdot; \phi)$.

3.1. Image Denoising Network for Gaussian Noise

We first train a denoising network by the standard supervised learning. Our denoising network, $\mathcal{D}(\cdot; \theta)$, aims to remove the Gaussian noise in an input image I and reconstruct a clean image close to the ground-truth I_{GT} . To achieve this, the model parameters θ are optimized by minimizing the following loss function:

$$\mathcal{L} = \|\mathcal{D}(I; \theta) - I_{\text{GT}}\|_1. \quad (2)$$

For training, the noisy input image I is corrupted by synthetic Gaussian noise. Detailed procedures for dataset construction are provided in Section 4.1.

3.2. Noise Translation Network

We now describe the training procedure for the noise translation network $\mathcal{T}(\cdot; \phi)$. During this phase, the parameters of the denoising network $\mathcal{D}(\cdot; \theta^*)$, trained for Gaussian noise removal, are kept fixed to provide a stable supervisory signal. The overall training pipeline is illustrated in Figure 3.

3.2.1. Implicit Noise Translation Loss

The objective is to transform an arbitrary noisy input image I into a noise-translated image $I_{\mathcal{T}}$ that is well-suited for the pretrained denoising network specialized in handling Gaussian noise. To this end, we optimize the noise translation network using the *implicit* noise translation loss, which minimizes the discrepancy between the denoised output and the corresponding clean ground-truth image:

$$\mathcal{L}_{\text{implicit}} = \|\hat{I}_{\mathcal{T}} - I_{\text{GT}}\|_1 = \|\mathcal{D}(\mathcal{T}(I; \phi); \theta^*) - I_{\text{GT}}\|_1. \quad (3)$$

This loss function encourages the translation network to map arbitrary unseen noise into a form that can be effectively handled by the pretrained Gaussian Denoiser $\mathcal{D}(\cdot; \theta^*)$. A natural choice for constructing training pairs (I, I_{GT}) for training the noise translation network is to use real noisy-clean image pairs. Accordingly, we exclusively use noisy-clean pairs from the real noise dataset SIDD [1].

3.2.2. Explicit Noise Translation Loss

Although the implicit noise translation loss encourages the translated image to be well-aligned with the pretrained denoising network, it does not explicitly enforce that the translated noise follows an ideal Gaussian distribution, as it lacks direct control over the noise characteristics. To address this, we introduce an explicit loss that promotes the translated noise to follow a Gaussian distribution.

Let $n_{\mathcal{T}} = I_{\mathcal{T}} - I_{GT} \in \mathbb{R}^{H \times W \times C}$ represent the translated noise, and let $n_{\mathcal{G}} \in \mathbb{R}^{H \times W \times C}$ be a random variable following a Gaussian distribution $\mathcal{N}(\hat{\mu}, \hat{\sigma}^2)$, where $\hat{\mu}$ and $\hat{\sigma}$ denote the empirical mean and standard deviation calculated from all elements of $n_{\mathcal{T}}$, respectively. We adjust the distribution of $n_{\mathcal{T}}$ to align with the distribution of $n_{\mathcal{G}}$. To this end, we employ the Wasserstein distance between the two distributions as a loss function, which is given by

$$\mathcal{L}_{\text{spatial}} \equiv d_{W_1}(n_{\mathcal{T}}, n_{\mathcal{G}}), \quad (4)$$

where $d_{W_1}(\cdot, \cdot)$ is 1-Wasserstein distance, also known as the Earth Mover’s Distance. To compute this, we first flatten each channel in $n_{\mathcal{T}}$ and $n_{\mathcal{G}}$ over the spatial dimensions into one-dimensional vectors, and then sort them in an ascending order. Let $\mathbf{X}^c \equiv (X_1^c, X_2^c, \dots, X_{H \times W}^c)$ and $\mathbf{Y}^c \equiv (Y_1^c, Y_2^c, \dots, Y_{H \times W}^c)$ denote the ordered values of $n_{\mathcal{T}}$ and $n_{\mathcal{G}}$ for the c^{th} channel, respectively. The 1-Wasserstein distance is then given by the following simple function¹:

$$d_{W_1}(n_{\mathcal{T}}, n_{\mathcal{G}}) = \frac{1}{H \cdot W \cdot C} \sum_{c=1}^C \sum_{i=1}^{H \cdot W} |X_{(i)}^c - Y_{(i)}^c|. \quad (5)$$

This loss encourages the translated noise $n_{\mathcal{T}}$ to follow a Gaussian distribution element-wise, but it is still insufficient to ensure that $n_{\mathcal{T}}$ is spatially uncorrelated. To handle the spatial correlation, we convert the signals of $n_{\mathcal{T}}$ and $n_{\mathcal{G}}$ into the frequency domain using their respective channel-wise Fourier transforms, which are given by

$$F_{\mathcal{T}}^c(u, v) = \sum_{x=0}^{H-1} \sum_{y=0}^{W-1} n_{\mathcal{T}}(x, y, c) e^{-2\pi i(\frac{ux}{H} + \frac{vy}{W})}, \quad (6)$$

$$F_{\mathcal{G}}^c(u, v) = \sum_{x=0}^{H-1} \sum_{y=0}^{W-1} n_{\mathcal{G}}(x, y, c) e^{-2\pi i(\frac{ux}{H} + \frac{vy}{W})}, \quad (7)$$

where (u, v) are the frequency domain coordinates and c is a channel index. Since $n_{\mathcal{G}}$ is spatially uncorrelated Gaussian noise, the real and imaginary parts of the Fourier coefficients, $F_{\mathcal{G}}^c(u, v)$, also follow *i.i.d.* Gaussian distributions with zero mean and the same variance. Consequently, the magnitude of the Fourier coefficients, $|F_{\mathcal{G}}^c(u, v)|$, follows a Rayleigh distribution as

$$p_R(|F_{\mathcal{G}}^c(u, v)|; \sigma) = \frac{|F_{\mathcal{G}}^c(u, v)|}{\sigma^2} \exp\left(-\frac{|F_{\mathcal{G}}^c(u, v)|^2}{2\sigma^2}\right), \quad (8)$$

which implies that $|F_{\mathcal{T}}^c(u, v)|$ should also follow a Rayleigh distribution, guiding $n_{\mathcal{T}}$ to be spatially uncorrelated. To this end, similar to Eqs. (4) and (5), we minimize the difference between the distributions of $|F_{\mathcal{T}}^c(u, v)|$ and $|F_{\mathcal{G}}^c(u, v)|$ by

¹Please refer to Appendix for the detailed proof.

utilizing 1-Wasserstein distance, which is defined as

$$\mathcal{L}_{\text{freq}} \equiv d_{W_1}(|F_{\mathcal{T}}|, |F_{\mathcal{G}}|) = \frac{1}{H \cdot W \cdot C} \sum_{c=1}^C \sum_{i=1}^{H \cdot W} |\tilde{X}_{(i)}^c - \tilde{Y}_{(i)}^c|, \quad (9)$$

where $\tilde{\mathbf{X}}^c \equiv (\tilde{X}_1^c, \tilde{X}_2^c, \dots, \tilde{X}_{H \times W}^c)$ and $\tilde{\mathbf{Y}}^c \equiv (\tilde{Y}_1^c, \tilde{Y}_2^c, \dots, \tilde{Y}_{H \times W}^c)$ are the sorted values of flattened magnitude of Fourier coefficients $|F_{\mathcal{T}}^c(u, v)|$ and $|F_{\mathcal{G}}^c(u, v)|$, respectively. The full explicit noise translation loss is defined by $\mathcal{L}_{\text{spatial}}$ and $\mathcal{L}_{\text{freq}}$ as

$$\mathcal{L}_{\text{explicit}} = \mathcal{L}_{\text{spatial}} + \beta \cdot \mathcal{L}_{\text{freq}}, \quad (10)$$

where β controls the contribution of the two Wasserstein distances. This loss function explicitly guides the translated noise to follow Gaussian distribution. The total loss function for training the noise translation network is given by

$$\mathcal{L}_{\text{total}} = \mathcal{L}_{\text{implicit}} + \alpha \cdot \mathcal{L}_{\text{explicit}}, \quad (11)$$

where α balances the influence of two loss terms.

3.2.3. Gaussian Injection Block

As shown in Figure 3, our noise translation network is based on a lightweight U-Net architecture, where each layer contains a Gaussian Injection Block (GIBlock). Each GIBlock combines a Nonlinear Activation-Free (NAF) block [6] with our key design, the injection of Gaussian noise, to consistently impose a Gaussian prior throughout the network.

While injecting Gaussian noise into the input can provide a Gaussian prior to some extent, it inevitably distorts the input signal. In contrast, our method injects Gaussian noise internally into sub-blocks of the network, allowing the network to receive the Gaussian prior gradually without perturbing the original image for translating unseen real noise effectively. Additionally, the residual connections between the input I and the output $I_{\mathcal{T}}$ further mitigate any signal distortion introduced by the injected noise. Ablation studies confirm that Gaussian noise injection is essential for enabling the noise translation network to reliably map unseen noise to a Gaussian distribution during inference.

4. Experiments

We demonstrate the effectiveness of the proposed approach on various benchmarks, evaluating performance and conducting analysis on both ID and OOD datasets. This section also provides an in-depth analysis of our algorithm, including detailed ablation studies and qualitative assessments.

4.1. Experimental Settings

Training details Our framework is model-agnostic and can be applied to various denoising networks. To demonstrate the effectiveness of the proposed approach, we adopt NAFNet [6] and Xformer [45], pretrained on BSD400 [29],

Table 1. Quantitative comparison with state-of-the-art real-world denoising networks on the SIDD validation set and various out-of-distribution (OOD) real-world benchmarks. The results are presented in terms of PSNR \uparrow (dB) and SSIM \uparrow . Models marked with an asterisk (*) are evaluated using official out-of-the-box models, while a dagger (\dagger) indicates models fine-tuned on the SIDD training dataset.

	Denoising Algo.	Metric	In-distribution			Out-of-distribution						
			SIDD	Poly	CC	HighISO	iPhone	Huawei	OPPO	Sony	Xiaomi	OOD Avg.
<i>Self-supervised</i>	R2R* [32]	PSNR	35.09	36.84	35.28	37.37	39.25	38.35	39.38	41.55	35.39	37.93
		SSIM	0.9154	0.9726	0.9758	0.9716	0.9614	0.9667	0.9744	0.9735	0.9668	0.9703
	AP-BSN* [19]	PSNR	36.35	35.91	33.15	36.70	39.90	37.06	39.11	40.13	33.39	36.92
		SSIM	0.9285	0.9755	0.9734	0.9781	0.9773	0.9633	0.9750	0.9805	0.9552	0.9723
	SSID* [21]	PSNR	37.43	37.17	34.95	38.28	40.95	37.27	39.17	43.03	34.27	38.14
		SSIM	0.9343	0.9803	0.9806	0.9811	0.9823	0.9656	0.9743	0.9883	0.9566	0.9762
	APR-RD* [16]	PSNR	38.06	37.01	35.83	38.75	40.40	36.75	38.93	43.35	33.74	38.10
		SSIM	0.9470	0.9781	0.9824	0.9823	0.9763	0.9590	0.9713	0.9861	0.9483	0.9730
<i>Generalization</i>	Mask-Denoising \dagger [5]	PSNR	38.91	37.45	35.64	38.12	40.54	37.99	39.55	44.04	35.12	38.56
		SSIM	0.9529	0.9808	0.9810	0.9793	0.9801	0.9694	0.9790	0.9899	0.9697	0.9786
	Clip-Denoising \dagger [8]	PSNR	38.03	37.49	35.92	38.26	40.27	38.07	39.73	43.42	35.11	38.53
		SSIM	0.9446	0.9795	0.9819	0.9782	0.9730	0.9702	0.9789	0.9857	0.9690	0.9771
	AFM* [34]	PSNR	38.29	37.71	36.81	39.12	40.56	38.33	40.13	44.66	35.25	39.07
		SSIM	0.9474	0.9800	0.9828	0.9797	0.9769	0.9679	0.9795	0.9901	0.9665	0.9745
	IDF \dagger [15]	PSNR	37.01	36.42	33.62	37.17	39.79	36.23	38.74	43.12	33.69	37.35
		SSIM	0.9354	0.9764	0.9754	0.9764	0.9771	0.9593	0.9754	0.9885	0.9563	0.9731
<i>Ours</i>	NAFNet* [6]	PSNR	39.97	37.17	35.69	38.32	40.25	37.73	39.64	43.65	34.99	38.43
		SSIM	0.9600	0.9717	0.9811	0.9788	0.9707	0.9680	0.9786	0.9829	0.9685	0.9750
	NAFNet + NTN	PSNR	39.24	38.72	37.84	40.00	42.08	39.83	40.55	44.34	36.17	39.94
		SSIM	0.9570	0.9855	0.9877	0.9856	0.9812	0.9782	0.9801	0.9875	0.9749	0.9826
	XFormer* [45]	PSNR	39.98	37.45	35.95	37.86	39.99	38.35	39.61	43.89	35.54	38.58
		SSIM	0.9603	0.9778	0.9782	0.9741	0.9732	0.9678	0.9779	0.9892	0.9706	0.9761
	XFormer + NTN	PSNR	39.10	38.75	37.82	40.29	42.20	39.89	40.70	44.44	36.25	40.04
		SSIM	0.9557	0.9856	0.9862	0.9860	0.9826	0.9779	0.9807	0.9886	0.9751	0.9828

WED [25], and SIDD-Medium [1] datasets. BSD400 and WED consist of clean images while SIDD provides real noisy-clean image pairs. During the training of a denoising network, noisy images are created by adding Gaussian noise with a standard deviation of 15 to clean images from BSD400 and WED and noisy images from SIDD. The noise translation network is trained subsequently, using SIDD images with data augmentation of random Gaussian noise sampled from $[0, 15]$. The hyperparameters are set as follows: a Gaussian noise level $\tilde{\sigma} = 100$, $\alpha = 5 \times 10^{-2}$, and $\beta = 2 \times 10^{-3}$. Additional training details such as batch size or training resources are discussed in Appendix.

Evaluation To evaluate the generalization performance of our framework, we employ various real-world image denoising benchmarks. We conduct experiments using SIDD validation dataset [1], Poly [38], CC [31], HighISO [40], iPhone, Huawei, Oppo, Sony, and Xiaomi [17]. The SIDD validation dataset consists of 256×256 images, while the Poly and CC datasets contain images with a resolution of 512×512 pixels. Images from HighISO, iPhone, Huawei, Oppo, Sony, and Xiaomi are 1024×1024 pixels in size.

4.2. Results

Performance on real noise Table 1 presents the performance of the proposed approach applied to existing de-

noising networks, NAFNet [6] and Xformer [45]. We also compare their results with those from self-supervised image denoising methods, including R2R [32], AP-BSN [19], SSID [21] and APR-RD [16] and generalizable image denoising methods, including Mask-Denoising [5], Clip-Denoising [8], AFM [34], and IDF [15]. We used the officially published, SIDD-pretrained models for comparisons if available. For the methods without such pretrained models such as Mask-Denoising, Clip-Denoising, and IDF, we trained these models on the SIDD training dataset until convergence to ensure a fair comparison.

As shown in Table 1, incorporating our noise translation framework, denoted by NAFNet + NTN and Xformer + NTN, achieves substantial average PSNR gains of 1.51dB and 1.46dB, respectively, in out-of-distribution (OOD) scenarios. Furthermore, our method demonstrates superior real-world image denoising generalization performance compared to other self-supervised and generalizable denoising methods. Additional comparisons—including LAN [14] applied to the same NAFNet architecture, as well as results on Restormer [43] and KNet [49] with NTN—are provided in the Appendix.

Qualitative results on OOD benchmarks Figure 4 illustrates qualitative results for denoising models on several real-world OOD datasets, including CC [31], and High-

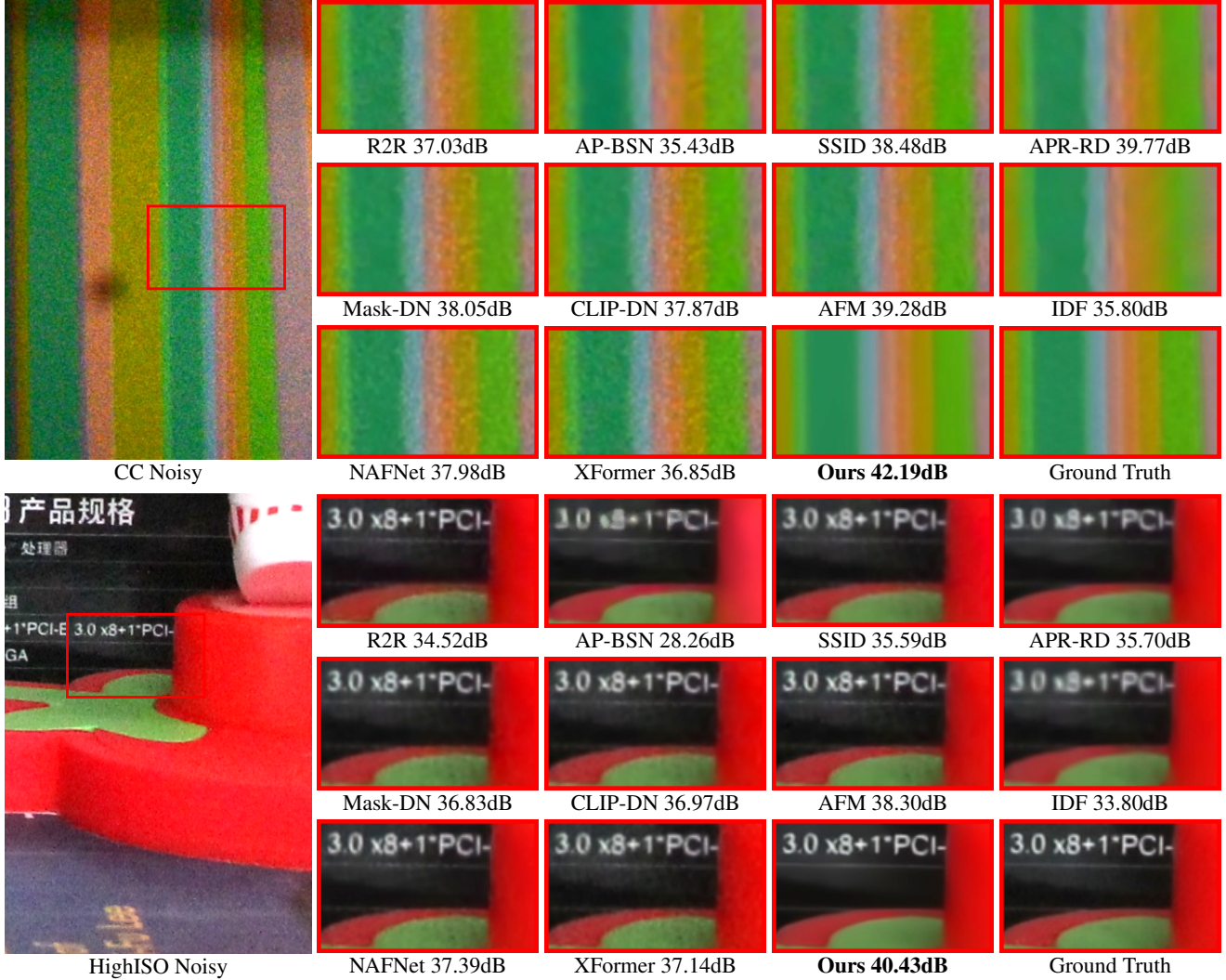


Figure 4. Comparison between the qualitative results of various denoising networks including ours (noise translation network with pre-trained NAFNet), on the out-of-distribution (OOD) datasets. Our result displays cleaner outputs compared to other state-of-the-art networks that are directly trained from a real-noise dataset. Zoom in for better comparison.

ISO [40]. Our model demonstrates significant superiority over other denoising methods in these challenging scenarios. Qualitative results on every benchmark listed in Table 1 are available in the Appendix.

4.3. Analysis

In this section, we present a comprehensive analysis using our noise translation network combined with a pretrained NAFNet as a denoising network (NAFNet + NTN).

Ablation study Table 2 presents the ablation study results of the proposed algorithm. The baseline model is trained using only the implicit noise translation loss, excluding both the Gaussian noise injection block (GIBlock) and the explicit noise translation loss. The results demonstrate that both components (GIBlock and explicit loss) are essential

Table 2. Ablation study of the Gaussian injection block (GIBlock) and the explicit noise translation loss. Full results on individual OOD datasets are provided in the Appendix.

	Metric	SIDD	OOD Avg.
Baseline translation	PSNR	39.35	39.27
	SSIM	0.9573	0.9774
+ GIBlock	PSNR	39.05	39.61
	SSIM	0.9556	0.9801
+ Explicit loss ($\mathcal{L}_{\text{explicit}}$)	PSNR	39.33	39.61
	SSIM	0.9572	0.9809
+ Both (Ours)	PSNR	39.24	39.94
	SSIM	0.9570	0.9826

for enhancing performance: GIBlock promotes the translation of complex noise into Gaussian noise, while the explicit loss provides a clear constraint that guides the generation toward *i.i.d.* Gaussian noise.

Table 3. Quantitative results based on variations in the noisy input to the pretrained denoising network on the in-distribution SIDD validation set and other out-of-distribution real-world benchmarks. I , $I + \mathcal{N}_5$, $I + \mathcal{N}_{10}$, and $I + \mathcal{N}_{15}$ represent the noisy input images with additional Gaussian noise levels of 0, 5, 10, and 15, respectively, which are fed into the pretrained Gaussian denoising network.

Input	Metric	In-distribution				Out-of-distribution					
		SIDD	Poly	CC	HighISO	iPhone	Huawei	OPPO	Sony	Xiaomi	OOD Avg.
I	PSNR	37.77	15.24	33.76	21.18	40.13	8.68	8.45	6.35	9.33	17.89
	SSIM	0.9360	0.3466	0.9139	0.5232	0.9734	0.1218	0.1138	0.0245	0.1845	0.4002
$I + \mathcal{N}_5$	PSNR	38.15	27.07	34.97	32.30	15.28	16.99	13.79	12.82	14.96	22.93
	SSIM	0.9436	0.7010	0.9211	0.8227	0.2392	0.3943	0.2564	0.1912	0.3540	0.5359
$I + \mathcal{N}_{10}$	PSNR	38.76	<u>38.27</u>	37.33	<u>39.40</u>	40.95	<u>39.44</u>	<u>39.98</u>	42.96	<u>35.91</u>	<u>39.22</u>
	SSIM	0.9536	0.9795	<u>0.9850</u>	<u>0.9825</u>	0.9638	<u>0.9762</u>	0.9768	0.9758	<u>0.9728</u>	0.9740
$I + \mathcal{N}_{15}$	PSNR	<u>39.16</u>	38.08	36.26	38.85	<u>41.12</u>	38.71	39.69	<u>43.42</u>	35.25	38.95
	SSIM	<u>0.9565</u>	<u>0.9834</u>	0.9829	0.9808	<u>0.9811</u>	0.9719	<u>0.9770</u>	0.9886	0.9680	<u>0.9767</u>
$I_{\mathcal{T}}$	PSNR	39.24	38.72	37.84	40.00	42.08	39.83	40.55	44.34	36.17	39.94
	SSIM	0.9570	0.9855	0.9877	0.9856	0.9812	0.9782	0.9801	<u>0.9875</u>	0.9749	0.9826

Table 4. Transferability of our noise translation network. Once trained with NAFNet [6], it integrates seamlessly with other denoising networks. We present performance only in PSNR \uparrow . Full results on each OOD dataset are provided in the Appendix.

\mathcal{D}_{θ^*} for testing	\mathcal{D}_{θ^*} for training \mathcal{T}_ϕ	SIDD	OOD Avg.
Xformer [45]	NAFNet [6]	39.17	39.94
	Xformer [45]	39.10	40.04

Comparisons with simple Gaussian noise additions We evaluate the effectiveness of our noise translation network by comparing it to directly adding Gaussian noise to the input. As shown in Table 3, simply adding Gaussian noise yields reasonable generalization. However, some datasets perform better with $I + \mathcal{N}_{10}$, while others with $I + \mathcal{N}_{15}$, indicating that noise characteristics vary across datasets or even individual images. This variation underscores the limitation of fixed noise and the need for a more adaptive approach. Our noise translation network can adaptively transform input noise into ideal Gaussian noise, achieving consistent performance gains across all datasets.

Transferability of noise translation network The noise translation network is functionally decoupled from the denoising network, allowing a single trained noise translation model to be paired with various pretrained denoising networks. Table 4 demonstrates this property by applying the noise translation network, trained with pretrained NAFNet [6], to other architecture, Xformer [45]. The performance remains comparable to that of individually trained noise translation networks for each denoiser. This suggests that a one-time trained noise translation network can generalize effectively across diverse pretrained denoising networks without additional training.

Analysis of translated noise Figure 5 visualizes the effect of our noise translation. Real noise shows strong spatial correlation, which our network effectively removes, pro-

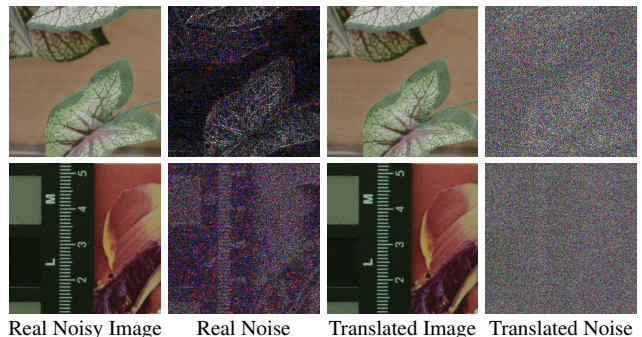


Figure 5. Visual results of noise translation. The noisy image in the top row is from the Poly [38] dataset, while the one in the bottom row is from the CC [31] dataset. For enhanced visualization, noise is displayed as the absolute value, scaled by a factor of 10.

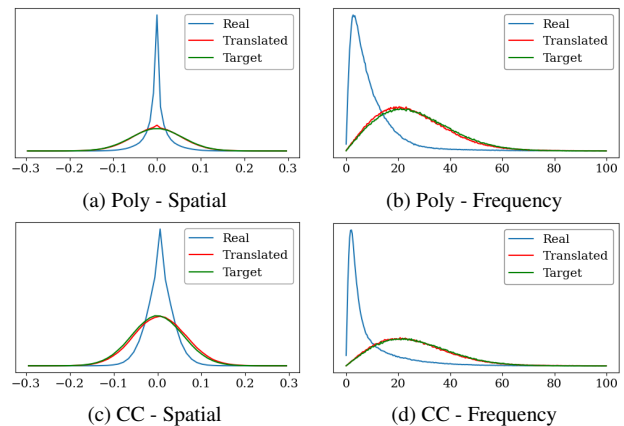


Figure 6. Histogram of noise distribution before (Real) and after noise translation network in both spatial and frequency domains. Target noise corresponds to the Gaussian noise with a level of 15, which the denoising network has been pretrained to remove.

ducing noise that closely resembles ideal Gaussian noise.

Figure 6 shows the noise distributions of the two images in Figure 5. In the spatial domain, ideal Gaussian noise fol-

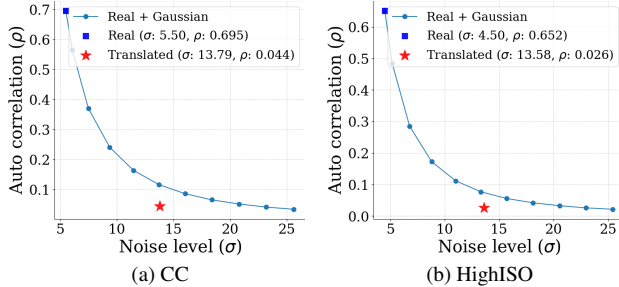


Figure 7. Analysis of noise characteristics. The blue curve illustrates the changes in noise level and auto-correlation resulting from adding various levels of Gaussian noise to the real noise. The results are averaged over the CC [31] and HighISO [40] datasets.

lows a normal distribution; in the frequency domain, it follows a Rayleigh distribution (see Section 3.2.2). Real noise significantly deviates from these targets, whereas translated noise closely matches them, demonstrating effective alignment with spatially uncorrelated, *i.i.d.* Gaussian noise.

Additionally, Figure 7 plots the noise level versus auto-correlation for each dataset, comparing three cases: (1) real noise, (2) real noise with added Gaussian noise, and (3) translated noise produced by our method. While adding Gaussian noise to real noise increases the overall noise level and reduces auto-correlation, our translated noise achieves substantially lower auto-correlation at comparable noise levels. This indicates that our translation process more effectively decorrelates the noise.

Evaluating Trade-offs in ID performance Figure 8 displays enlarged qualitative results on the SIDD validation dataset. Although our method may appear to exhibit a trade-off in in-distribution performance, this primarily stems from the pronounced overfitting of other models, which often reconstruct irrelevant artifacts inherent in the training data. In contrast, our approach avoids such overfitting while still producing high-quality reconstructions.

If improving in-distribution performance on a specific dataset is desired, the denoising network can be fine-tuned. We demonstrate this by freezing the trained translation network and fine-tuning only the denoising network on the SIDD dataset. As shown in Table 5, this procedure yields an improvement of approximately 0.3dB on SIDD while having negligible impact on out-of-distribution performance.

Computational efficiency Table 6 presents a comparison of our noise translation network with other image denoising networks including NAFNet [6] and Xformer [45] in terms of the number of parameters and multiply-accumulate operations (MACs). Our noise translation network is substantially smaller in both parameter count and MACs than the image denoising networks, adding only negligible computational overhead during inference.

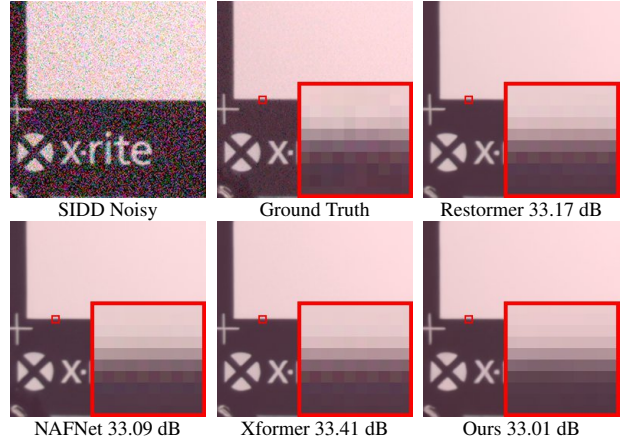


Figure 8. Denoised results of an in-distribution SIDD [1] noisy image. Only our approach effectively avoids overfitting, preventing unnecessary zipper artifacts prevalent in the training set, while preserving the visual quality. Zoom in for detailed comparison.

Table 5. Impact of SIDD [1] fine-tuning. We present the performance of NAFNet and Xformer when the noise translation network is frozen and only the denoising network is fine-tuned.

		Metric	SIDD	OOD Avg.
NAFNet + NTNet	PSNR		39.56 (+0.32)	39.95 (+0.01)
	SSIM		0.9580 (+0.001)	0.9830 (+0.0004)
Xformer + NTNet	PSNR		39.43 (+0.33)	39.97 (-0.07)
	SSIM		0.9589 (+0.0032)	0.9903 (+0.0075)

Table 6. Parameter counts and MACs of denoising networks and our noise translation network. We report the number of parameters and MACs at inference, estimated with an input size of 256×256 .

Architecture	Parameters (M)	MACs (G)
NAFNet [6]	29.10	16.23
Xformer [45]	25.12	142.68
Noise Translation Network	0.29	1.07

5. Conclusion

We presented a novel noise translation framework for robust image denoising. Our framework allows us to effectively remove various unseen real noise, even with a limited amount of training data. By employing the noise translation network, arbitrary out-of-distribution (OOD) noise is translated into Gaussian noise for which an image denoising network has learned during training. The noise translation network is designed with well-motivated loss functions and architecture, enabling effective noise translation while preserving image contents. Our experiments demonstrate that the proposed approach significantly outperforms state-of-the-art denoising models in diverse OOD real-noise benchmarks. Finally, we highlight that the generalization issue in real-world scenarios remains a critical challenge in image denoising, and our approach offers a promising solution.

Acknowledgements This work was supported by the National Research Foundation of Korea (NRF) [RS-2022-NR070855, Trustworthy Artificial Intelligence] and the Institute of Information & Communications Technology Planning & Evaluation (IITP) [RS2022-II220959 (No.2022-0-00959), (Part 2) Few-Shot Learning of Causal Inference in Vision and Language for Decision Making; RS-2025-25442338, AI star Fellowship Support Program (Seoul National Univ.); No.RS-2021-II211343, Artificial Intelligence Graduate School Program (Seoul National University)], funded by the Korea government (MSIT).

References

- [1] Abdelrahman Abdelhamed, Stephen Lin, and Michael S Brown. A high-quality denoising dataset for smartphone cameras. In *CVPR*, 2018. 1, 2, 3, 5, 8
- [2] Joshua Batson and Loic Royer. Noise2self: Blind denoising by self-supervision. In *ICML*, 2019. 2
- [3] Benoit Brummer and Christophe De Vleeschouwer. Natural image noise dataset. In *CVPRW*, 2019. 1, 15
- [4] Yuanhao Cai, Xiaowan Hu, Haoqian Wang, Yulun Zhang, Hanspeter Pfister, and Donglai Wei. Learning to generate realistic noisy images via pixel-level noise-aware adversarial training. In *NeurIPS*, 2021. 2, 12
- [5] Haoyu Chen, Jinjin Gu, Yihao Liu, Salma Abdel Magid, Chao Dong, Qiong Wang, Hanspeter Pfister, and Lei Zhu. Masked image training for generalizable deep image denoising. In *CVPR*, 2023. 2, 5, 12
- [6] Liangyu Chen, Xiaojie Chu, Xiangyu Zhang, and Jian Sun. Simple baselines for image restoration. In *ECCV*, 2022. 1, 2, 4, 5, 7, 8, 12, 13, 14
- [7] Zheng Chen, Kai Liu, Jue Gong, Jingkai Wang, Lei Sun, Zongwei Wu, Radu Timofte, et al. Ntire 2025 challenge on image super-resolution (x4): Methods and results. In *CVPRW*, 2025. 2
- [8] Jun Cheng, Dong Liang, and Shan Tan. Transfer clip for generalizable image denoising. In *CVPR*, 2024. 2, 5, 12
- [9] Shuhang Gu, Yawei Li, Luc Van Gool, and Radu Timofte. Self-guided network for fast image denoising. In *ICCV*, 2019. 2
- [10] Shi Guo, Zifei Yan, Kai Zhang, Wangmeng Zuo, and Lei Zhang. Toward convolutional blind denoising of real photographs. In *CVPR*, 2019. 1
- [11] Tao Huang, Songjiang Li, Xu Jia, Huchuan Lu, and Jianzhuang Liu. Neighbor2neighbor: Self-supervised denoising from single noisy images. In *CVPR*, 2021. 2
- [12] Geonwoon Jang, Wooseok Lee, Sanghyun Son, and Kyoung Mu Lee. C2n: Practical generative noise modeling for real-world denoising. In *ICCV*, 2021. 2, 12
- [13] Junoh Kang, Donghun Ryou, and Bohyung Han. Icm-sr: Image-conditioned manifold regularization for image super-resolution. *arXiv preprint arXiv:2511.22048*, 2025. 2
- [14] Changjin Kim, Tae Hyun Kim, and Sungyong Baik. Lan: Learning to adapt noise for image denoising. In *CVPR*, 2024. 3, 5, 12, 13
- [15] Dongjin Kim, Jaekyun Ko, Muhammad Kashif Ali, and Tae Hyun Kim. Idf: Iterative dynamic filtering networks for generalizable image denoising. In *ICCV*, 2025. 2, 5, 12
- [16] Hyunjun Kim and Nam Ik Cho. Apr-rd: Complemental two steps for self-supervised real image denoising. In *AAAI*, 2025. 5
- [17] Zhaoming Kong, Fangxi Deng, Haomin Zhuang, Jun Yu, Lifang He, and Xiaowei Yang. A comparison of image denoising methods. *arXiv preprint arXiv:2304.08990*, 2023. 5
- [18] Alexander Krull, Tim-Oliver Buchholz, and Florian Jug. Noise2void-learning denoising from single noisy images. In *CVPR*, 2019. 2
- [19] Wooseok Lee, Sanghyun Son, and Kyoung Mu Lee. Ap-bsn: Self-supervised denoising for real-world images via asymmetric pd and blind-spot network. In *CVPR*, 2022. 5
- [20] Jaakko Lehtinen, Jacob Munkberg, Jon Hasselgren, Samuli Laine, Tero Karras, Miika Aittala, and Timo Aila. Noise2noise: Learning image restoration without clean data. In *ICML*, 2018. 2
- [21] Junyi Li, Zhilu Zhang, Xiaoyu Liu, Chaoyu Feng, Xiaotao Wang, Lei Lei, and Wangmeng Zuo. Spatially adaptive self-supervised learning for real-world image denoising. In *CVPR*, 2023. 2, 5
- [22] Ding Liu, Bihan Wen, Yuchen Fan, Chen Change Loy, and Thomas S Huang. Non-local recurrent network for image restoration. In *NeurIPS*, 2018. 2
- [23] Xing Liu, Masanori Suganuma, Zhun Sun, and Takayuki Okatani. Dual residual networks leveraging the potential of paired operations for image restoration. In *CVPR*, 2019. 2
- [24] Ilya Loshchilov and Frank Hutter. Decoupled weight decay regularization. In *ICLR*, 2019. 11
- [25] Kede Ma, Zhengfang Duanmu, Qingbo Wu, Zhou Wang, Hongwei Yong, Hongliang Li, and Lei Zhang. Waterloo exploration database: New challenges for image quality assessment models. *IEEE Transactions on Image Processing*, 26(2), 2016. 5
- [26] Markku Makitalo and Alessandro Foi. Optimal inversion of the generalized anscombe transformation for poisson-gaussian noise. *IEEE transactions on image processing*, 22(1):91–103, 2012. 3
- [27] Youssef Mansour and Reinhard Heckel. Zero-shot noise2noise: Efficient image denoising without any data. In *CVPR*, 2023. 2
- [28] Xiaojiao Mao, Chunhua Shen, and Yu-Bin Yang. Image restoration using very deep convolutional encoder-decoder networks with symmetric skip connections. In *NeurIPS*, 2016. 1
- [29] David Martin, Charless Fowlkes, Doron Tal, and Jitendra Malik. A database of human segmented natural images and its application to evaluating segmentation algorithms and measuring ecological statistics. In *ICCV*, 2001. 4
- [30] Sreyas Mohan, Zahra Kadkhodaie, Eero P. Simoncelli, and Carlos Fernandez-Granda. Robust and interpretable blind image denoising via bias-free convolutional neural networks. In *ICLR*, 2020. 2
- [31] Seonghyeon Nam, Youngbae Hwang, Yasuyuki Matsushita, and Seon Joo Kim. A holistic approach to cross-channel im-

- age noise modeling and its application to image denoising. In *CVPR*, 2016. 5, 7, 8
- [32] Tongyao Pang, Huan Zheng, Yuhui Quan, and Hui Ji. Recorrupted-to-recorrupted: unsupervised deep learning for image denoising. In *CVPR*, 2021. 2, 5
- [33] Yuhui Quan, Mingqin Chen, Tongyao Pang, and Hui Ji. Self2self with dropout: Learning self-supervised denoising from single image. In *CVPR*, 2020. 2
- [34] Donghun Ryou, Inju Ha, Hyewon Yoo, Dongwan Kim, and Bohyung Han. Robust image denoising through adversarial frequency mixup. In *CVPR*, 2024. 2, 5, 12, 13
- [35] Donghun Ryou, Inju Ha, Sanghyeok Chu, and Bohyung Han. Beyond the ground truth: Enhanced supervision for image restoration. In *CVPR*, 2026. 2
- [36] Lei Sun, Hang Guo, Bin Ren, Luc Van Gool, Radu Timofte, and Yawei Li. The tenth ntire 2025 image denoising challenge report. In *CVPRW*, 2025. 1
- [37] C. Villani and American Mathematical Society. *Topics in Optimal Transportation*. American Mathematical Society, 2003. 11
- [38] Jun Xu, Hui Li, Zhetong Liang, David Zhang, and Lei Zhang. Real-world noisy image denoising: A new benchmark. *arXiv preprint arXiv:1804.02603*, 2018. 1, 2, 5, 7
- [39] Hanshu Yan, Jingfeng Zhang, Jiashi Feng, Masashi Sugiyama, and Vincent YF Tan. Towards adversarially robust deep image denoising. In *IJCAI*, 2022. 2
- [40] Huanjing Yue, Jianjun Liu, Jingyu Yang, Truong Q Nguyen, and Feng Wu. High iso jpeg image denoising by deep fusion of collaborative and convolutional filtering. *IEEE Transactions on Image Processing*, 28(9), 2019. 1, 2, 5, 6, 8
- [41] Zongsheng Yue, Qian Zhao, Lei Zhang, and Deyu Meng. Dual adversarial network: Toward real-world noise removal and noise generation. In *ECCV*, 2020. 2, 12
- [42] Syed Waqas Zamir, Aditya Arora, Salman Khan, Munawar Hayat, Fahad Shahbaz Khan, Ming-Hsuan Yang, and Ling Shao. Learning enriched features for real image restoration and enhancement. In *ECCV*, 2020. 1
- [43] Syed Waqas Zamir, Aditya Arora, Salman Khan, Munawar Hayat, Fahad Shahbaz Khan, and Ming-Hsuan Yang. Restormer: Efficient transformer for high-resolution image restoration. In *CVPR*, 2022. 2, 5, 11, 12, 13, 14, 15
- [44] Syed Waqas Zamir, Aditya Arora, Salman Khan, Munawar Hayat, Fahad Shahbaz Khan, Ming-Hsuan Yang, and Ling Shao. Learning enriched features for fast image restoration and enhancement. *IEEE transactions on pattern analysis and machine intelligence*, 45(2), 2022.
- [45] Jiale Zhang, Yulun Zhang, Jinjin Gu, Jiahua Dong, Linghe Kong, and Xiaokang Yang. Xformer: Hybrid x-shaped transformer for image denoising. In *ICLR*, 2024. 2, 4, 5, 7, 8, 12
- [46] Kai Zhang, Wangmeng Zuo, Yunjin Chen, Deyu Meng, and Lei Zhang. Beyond a gaussian denoiser: Residual learning of deep cnn for image denoising. *IEEE transactions on image processing*, 26(7), 2017. 1, 2
- [47] Kai Zhang, Wangmeng Zuo, and Lei Zhang. Ffdnet: Toward a fast and flexible solution for cnn-based image denoising. *IEEE Transactions on Image Processing*, 27(9), 2018. 1
- [48] Yulun Zhang, Kunpeng Li, Kai Li, Bineng Zhong, and Yun Fu. Residual non-local attention networks for image restoration. In *ICLR*, 2019. 2
- [49] Yi Zhang, Dasong Li, Xiaoyu Shi, Dailan He, Kangning Song, Xiaogang Wang, Honwei Qin, and Hongsheng Li. Kbnnet: Kernel basis network for image restoration. *arXiv preprint arXiv:2303.02881*, 2023. 5, 11, 12
- [50] Yuqian Zhou, Jianbo Jiao, Haibin Huang, Yang Wang, Jue Wang, Honghui Shi, and Thomas Huang. When awgn-based denoiser meets real noises. In *AAAI*, 2020. 3, 12

Learning to Translate Noise for Robust Image Denoising

Supplementary Material

6. Proof on Wasserstein Distance

Let P and Q represent two probability distributions over \mathbb{R}^d . We use $X \sim P$ and $Y \sim Q$ to denote random variables with the distributions P and Q , respectively. The p -Wasserstein distance between two probability measures P and Q is defined as follows:

$$W_p(P, Q) = \left(\inf_{J \in \mathcal{J}(P, Q)} \int \|x - y\|^p dJ(x, y) \right)^{1/p}, \quad (12)$$

where $\mathcal{J}(P, Q)$ is the set of all joint distributions (or couplings) J on (X, Y) that have marginals P and Q . This formulation describes the minimum cost of transporting mass from distribution P to distribution Q using the coupling J , with the cost measured as the p -th power of the distance between points x and y .

In the Monge formulation, the goal is to find a transport map $T : \mathbb{R}^d \rightarrow \mathbb{R}^d$ such that the push-forward of P under T , denoted as $T_{\#}P$, equals Q . This problem can be mathematically formulated as:

$$\inf_T \int |x - T(x)|^p dP(x), \quad (13)$$

where the map T moves the distribution P to Q . However, an optimal map T may not always exist. In such cases, the Kantorovich formulation is used, allowing mass at each point to be split and transported to multiple locations, leading to a coupling-based approach.

For the specific case of $p = 1$, known as the Earth Mover’s Distance, the dual formulation of the Wasserstein distance can be expressed as:

$$W_1(P, Q) = \sup_{f \in F} \left(\int f(x) dP(x) - \int f(x) dQ(x) \right), \quad (14)$$

where F represents the set of all Lipschitz continuous functions $f : \mathbb{R}^d \rightarrow \mathbb{R}$ such that $|f(y) - f(x)| \leq \|x - y\|$ for all $x, y \in \mathbb{R}^d$. Then, the 1-Wasserstein distance is given by:

$$W_1(P, Q) = \int_0^1 |F^{-1}(z) - G^{-1}(z)| dz, \quad (15)$$

where F^{-1} and G^{-1} denote the quantile functions (inverse CDFs) of P and Q , respectively.

*indicates equal contribution.

When P and Q are empirical distributions based on the datasets, X_1, X_2, \dots, X_n and Y_1, Y_2, \dots, Y_n , each of size n , the Wasserstein distance can be computed as a function of the order statistics:

$$W_1(P, Q) = \sum_{i=1}^n |X_{(i)} - Y_{(i)}|, \quad (16)$$

where $X_{(i)}$ and $Y_{(i)}$ denote the i -th order statistics of the datasets X_1, X_2, \dots, X_n and Y_1, Y_2, \dots, Y_n .

In our approach, we utilize (16) to formulate $\mathcal{L}_{\text{spatial}}$ in Eq. (5) and $\mathcal{L}_{\text{freq}}$ in Eq. (10), which are employed during training to explicitly transport the translated noise distribution towards the target Gaussian distribution. We refer to [37] for a detailed discussion on Wasserstein distances and optimal transport.

7. Additional training details

The denoising models are trained for 200K iterations with a batch size of 32, except for Restormer and Xformer, where the batch size is reduced to 4 due to the limitation of computational resources. The noise translation network is trained for 5K iterations with a batch size of 4. The explicit noise translation loss was adopted only after half (2.5k) iterations, as early translated noise exhibits large deviations that destabilize optimization. Denoising network and noise translation network are trained with the AdamW [24] optimizer with an initial learning rate of 10^{-3} , which is reduced to 10^{-7} and 10^{-5} by a cosine annealing schedule, respectively. Each image is randomly cropped to 256×256 for training. All trainings were conducted using two NVIDIA RTX A6000 GPUs.

8. Additional experimental results

8.1. Model-agnostic applicability

To demonstrate the model-agnostic nature of our proposed noise translation framework, we applied our method to distinct architectural paradigms, specifically the transformer-based Restormer [43] and the kernel-based KBNNet [49], as noted in the main paper. Integrating our training framework into these baselines yielded consistent performance improvements in real-world denoising tasks, as detailed in Table 7. These results verify that our approach is not tailored to a specific backbone network but functions as a highly compatible framework capable of boosting the performance of diverse denoising architectures.

Table 7. Demonstration of model-agnostic applicability. We compare representative state-of-the-art denoising networks with their counterparts integrated with our proposed framework (+ NTN). The results are presented in terms of PSNR \uparrow (dB) and SSIM \uparrow . Models marked with an asterisk (*) are evaluated using official out-of-the-box models.

Denoising Algo.	Metric	In-distribution				Out-of-distribution					
		SIDD	Poly	CC	HighISO	iPhone	Huawei	OPPO	Sony	Xiaomi	OOD Avg.
Restormer* [43]	PSNR	40.02	37.66	36.33	38.29	40.13	38.42	39.56	44.19	35.65	38.78
	SSIM	0.9603	0.9793	0.9807	0.9756	0.9734	0.9675	0.9773	0.9894	0.9710	0.9768
Restormer + NTN	PSNR	39.22	38.76	37.68	40.14	41.85	39.72	40.64	44.29	36.19	39.91
	SSIM	0.9569	0.9854	0.9866	0.9857	0.9786	0.9766	0.9800	0.9871	0.9750	0.9819
NAFNet* [6]	PSNR	39.97	37.17	35.69	38.32	40.25	37.73	39.64	43.65	34.99	38.43
	SSIM	0.9600	0.9717	0.9811	0.9788	0.9707	0.9680	0.9786	0.9829	0.9685	0.9750
NAFNet + NTN	PSNR	39.24	38.72	37.84	40.00	42.08	39.83	40.55	44.34	36.17	39.94
	SSIM	0.9570	0.9855	0.9877	0.9856	0.9812	0.9782	0.9801	0.9875	0.9749	0.9826
KBNet* [49]	PSNR	40.35	36.82	35.23	38.09	38.00	35.18	37.80	41.79	34.25	37.15
	SSIM	0.9623	0.9789	0.9810	0.9788	0.9533	0.9462	0.9663	0.9790	0.9644	0.9685
KBNet + NTN	PSNR	39.13	38.62	37.61	39.89	41.76	39.80	40.57	44.22	36.07	39.82
	SSIM	0.9564	0.9843	0.9861	0.9849	0.9761	0.9777	0.9798	0.9845	0.9743	0.9810
XFormer* [45]	PSNR	39.98	37.45	35.95	37.86	39.99	38.35	39.61	43.89	35.54	38.58
	SSIM	0.9603	0.9778	0.9782	0.9741	0.9732	0.9678	0.9779	0.9892	0.9706	0.9761
XFormer + NTN	PSNR	39.10	38.75	37.82	40.29	42.20	39.89	40.70	44.44	36.25	40.04
	SSIM	0.9557	0.9856	0.9862	0.9860	0.9826	0.9779	0.9807	0.9886	0.9751	0.9828

Table 8. Quantitative comparison of additional state-of-the-art image denoising methods on the SIDD validation set and multiple real-noise benchmarks. We present the results in terms of PSNR \uparrow (dB) and SSIM \uparrow . Methods marked with an asterisk (*) are evaluated using official out-of-the-box models.

Denoising method		Metric	SIDD	Poly	CC	HighISO	iPhone	Huawei	OPPO	Sony	Xiaomi	Total Avg.
GAN-based	DANet* [41]	PSNR	39.47	37.53	36.16	38.35	40.46	38.40	39.85	44.36	35.57	38.90
		SSIM	0.9570	0.9800	0.9815	0.9770	0.9751	0.9691	0.9789	0.9895	0.9706	0.9754
	C2N + DIDN* [12]	PSNR	35.36	37.60	36.92	38.82	40.48	38.56	40.08	44.63	35.44	38.65
		SSIM	0.9321	0.9781	0.9813	0.9765	0.9745	0.9679	0.9793	0.9899	0.9684	0.9720
	PNGAN + MIRNet* [4]	PSNR	39.98	37.41	36.10	38.24	39.93	38.02	39.56	43.15	35.24	38.62
		SSIM	0.959	0.9783	0.9810	0.9763	0.9711	0.9678	0.9782	0.9860	0.9690	0.9741
Others	PDDenoising* [50]	PSNR	33.95	37.10	35.82	37.09	39.13	37.69	38.75	43.60	35.03	37.57
		SSIM	0.8986	0.9716	0.9742	0.9628	0.9611	0.9592	0.9707	0.9866	0.9626	0.9608
	CLIPDenoising* [8]	PSNR	34.79	37.54	36.30	38.01	40.09	38.74	39.56	42.94	35.50	38.16
		SSIM	0.8982	0.9794	0.9809	0.9771	0.9685	0.9715	0.9769	0.9824	0.9707	0.9672
	MaskDenoising* [5]	PSNR	28.66	34.56	33.87	34.61	36.54	34.89	35.30	37.89	33.46	34.42
		SSIM	0.7127	0.9553	0.9703	0.9649	0.9273	0.9586	0.9593	0.9354	0.9531	0.9263
IDF* [15]	PSNR	31.73	37.22	36.14	37.50	40.36	37.77	38.64	42.58	34.95	37.43	
	SSIM	0.8011	0.9790	0.9809	0.9759	0.9776	0.9649	0.9728	0.9848	0.9617	0.9554	
Ours	NAFNet + NTN	PSNR	39.24	38.72	37.84	40.00	42.08	39.83	40.55	44.34	36.17	39.86
		SSIM	0.9570	0.9855	0.9877	0.9856	0.9812	0.9782	0.9801	0.9875	0.9749	0.9797

8.2. Comparison with additional denoising methods

Table 8 presents quantitative comparisons between additional image denoising methods and our approach. Generation-based methods such as DANet [41], C2N [12], and PNGAN [4] utilize the SIDD dataset for training, focusing on synthetic-to-real noise generation. PDDenoising [50] applies pixel-shuffle down-sampling to denoise complex real noise with a simple Gaussian denoiser. However, pixel-shuffling alters image semantics, and optimal shuffling parameters vary per image, making optimization challenging and yielding poor performance. MaskDenoising [5] and IDF [15] are trained solely on Gaussian noise ($\sigma = 15$), leading to notably poor performance on real-world noise datasets. CLIPDenoising [8] leverages the CLIP encoder and incorporates additional training on synthetic noise generated using Poisson-Gaussian models for sRGB denoising.

However, none of these methods outperform our approach across most benchmarks, underscoring the efficacy of our noise translation framework in handling real-world noise scenarios.

8.3. Comparison with generalization methods

Table 9 showcases results from our reproduction of the AFM [34] and LAN [14] methods using their officially released code, in combination with NAFNet, to enable a direct comparison with our proposed method. Applying LAN to other denoising architectures from our experiments, such as Restormer [43], KBNet [49], and Xformer [45], was infeasible due to excessive memory demands of LAN when processing images with resolutions exceeding 512×512 . Additionally, our reproduction experiments revealed that LAN’s adaptation methodology not only requires substantial computational resources but also fails to improve

Table 9. Quantitative comparisons with state-of-the-art generalization methods on the SIDD validation set and multiple real-noise benchmarks. We present the results in terms of PSNR \uparrow (dB) and SSIM \uparrow . Methods marked with a dagger (\dagger) indicate evaluations performed on reproduced models under standardized conditions.

Baseline	Generalization	Metric	In-distribution				Out-of-distribution					
			SIDD	Poly	CC	HighISO	iPhone	Huawei	OPPO	Sony	Xiaomi	OOD Avg.
NAFNet [6]	None	PSNR	39.97	37.17	35.69	38.32	40.25	37.73	39.64	43.65	34.99	38.43
		SSIM	0.9600	0.9717	0.9811	0.9788	0.9707	0.9680	0.9786	0.9829	0.9685	0.9750
	+ AFM \dagger [34]	PSNR	39.83	37.28	36.31	38.40	39.68	38.21	39.84	43.31	35.39	38.55
		SSIM	0.9592	0.9696	0.9815	0.9783	0.9545	0.9683	0.9788	0.9637	0.9709	0.9707
	+ LAN \dagger [14]	PSNR	39.88	37.17	35.59	38.21	40.48	37.53	39.42	43.66	34.83	38.36
		SSIM	0.9594	0.9792	0.9808	0.9787	0.9766	0.9680	0.9773	0.9883	0.9667	0.9770
	+ NTN	PSNR	39.24	38.72	37.84	40.00	42.08	39.83	40.55	44.34	36.17	39.94
		SSIM	0.9570	0.9855	0.9877	0.9856	0.9812	0.9782	0.9801	0.9875	0.9749	0.9826

Table 10. Expanded table of Table 2: Gaussian injection and explicit noise translation loss.

	Metric	In-distribution				Out-of-distribution					
		SIDD	Poly	CC	HighISO	iPhone	Huawei	OPPO	Sony	Xiaomi	OOD Avg.
w/o GIBlock	PSNR	39.35	38.32	37.25	39.22	40.80	39.24	39.75	43.86	35.74	39.27
	SSIM	0.9573	0.9820	0.9864	0.9794	0.9700	0.9727	0.9745	0.9857	0.9683	0.9774
w/o Explicit Loss	PSNR	39.05	38.54	37.58	39.79	41.53	39.68	40.40	43.89	36.00	39.61
	SSIM	0.9556	0.9835	0.9866	0.9844	0.9737	0.9773	0.9790	0.9827	0.9737	0.9801
w/o adaptive gating ($\mathcal{L}_{\text{explicit}}$)	PSNR	39.33	38.59	37.10	39.35	41.69	39.56	40.27	44.34	35.95	39.61
	SSIM	0.9572	0.9846	0.9864	0.9821	0.9793	0.9753	0.9782	0.9888	0.9720	0.9808
Full (Ours)	PSNR	39.24	38.72	37.84	40.00	42.08	39.83	40.55	44.34	36.17	39.94
	SSIM	0.9570	0.9855	0.9877	0.9856	0.9812	0.9782	0.9801	0.9875	0.9749	0.9826

generalization performance at resolutions exceeding 256×256 . In contrast, our noise translation framework consistently delivers robust and superior generalization performance across diverse out-of-distribution benchmarks, outperforming both AFM and LAN.

8.4. Expanded Table: Gaussian Injection Block and Explicit Noise Translation Loss

Table 10 provides the complete results for the OOD benchmarks in Table 2 of the main paper. These results further demonstrate the effectiveness of the Gaussian injection block and explicit noise translation loss within the proposed framework.

8.5. Expanded Table: Adaptability of the Noise Translation Network

Table 11 extends the results of Table 4 in the main paper, analyzing various combinations of denoising networks used during the training and inference phases within our framework. In this context, \mathcal{D}_{θ^*} for testing refers to the pretrained denoising network utilized during inference, while \mathcal{D}_{θ^*} for training \mathcal{T}_{ϕ} denotes the pretrained denoising network employed for training the noise translation network. For instance, when \mathcal{D}_{θ^*} for testing is NAFNet and \mathcal{D}_{θ^*} for training \mathcal{T}_{ϕ} is KBNNet, the noise translation network is trained to map real-world noise to align with KBNNet’s prior but is evaluated with NAFNet during inference. Notably, when \mathcal{D}_{θ^*} for testing and \mathcal{D}_{θ^*} for training \mathcal{T}_{ϕ} correspond to different pretrained denoising models, our framework maintains high performance by effectively translating noise distributions to align with the priors of the inference model. This

adaptability implies that as new denoising architectures are introduced, they can be seamlessly incorporated into our framework, potentially achieving even greater performance improvements without the need to retrain the noise translation network. Such flexibility ensures the practical applicability of our noise translation framework in real-world scenarios.

8.6. Comparison with naïve combination of real and synthetic dataset for training

We compare our method with the naïve approach of combining Gaussian noise dataset with the SIDD dataset for training. The results are presented in Table 12. The Gaussian noise dataset used in this comparison is identical to the one which is used for our method. The results demonstrate that naïvely combining real-noise and Gaussian noise datasets during training does not yield significant improvements in generalization performance. This highlights the superiority and efficacy of our method in enhancing denoising performance across diverse noise distributions.

8.7. Incorporating a pure Gaussian pretrained denoising network

We conduct an experiment on the officially published denoising model, Restormer [43], which was trained for blind gaussian noise removal. By leveraging it in our framework, we trained the corresponding noise translation network with the proposed methodology to evaluate the overall performance. The results are provided in Table 13, which demonstrate that even when using a pure Gaussian pretrained out-of-the-box model within our framework, the real-world de-

Table 11. Expanded table of Table 4: Adaptability of the noise translation network.

\mathcal{D}_{θ^*} for testing	\mathcal{D}_{θ^*} for training	\mathcal{T}_{ϕ}	Metric	In-distribution			Out-of-distribution						OOD Avg.
				SIDD	Poly	CC	HighISO	iPhone	Huawei	OPPO	Sony	Xiaomi	
Restormer	Restormer	PSNR	39.22	38.76	37.68	40.14	41.85	39.72	40.64	44.29	36.19	39.91	
		SSIM	0.9569	0.9854	0.9866	0.9857	0.9786	0.9766	0.9800	0.9871	0.9750	0.9819	
	NAFNet	PSNR	39.16	38.65	37.34	39.98	41.92	39.73	40.56	43.95	36.19	39.79	
		SSIM	0.9564	0.9851	0.9861	0.9854	0.9811	0.9770	0.9800	0.9871	0.9750	0.9821	
	KBNet	PSNR	39.21	38.53	37.05	39.88	41.93	39.65	40.53	43.81	36.14	39.69	
		SSIM	0.9567	0.9848	0.9851	0.9850	0.9817	0.9766	0.9799	0.9873	0.9743	0.9819	
	Xformer	PSNR	39.12	38.73	37.80	40.11	41.65	39.64	40.42	44.11	36.18	39.83	
		SSIM	0.9559	0.9850	0.9867	0.9852	0.9774	0.9763	0.9795	0.9866	0.9746	0.9814	
NAFNet	Restormer	PSNR	39.16	38.61	38.00	40.07	41.95	39.71	40.41	44.05	36.22	39.88	
		SSIM	0.9565	0.9846	0.9877	0.9856	0.9800	0.9775	0.9793	0.9858	0.9748	0.9819	
	NAFNet	PSNR	39.24	38.72	37.84	40.00	42.08	39.83	40.55	44.34	36.17	39.94	
		SSIM	0.9570	0.9855	0.9877	0.9856	0.9812	0.9782	0.9801	0.9875	0.9749	0.9826	
	KBNet	PSNR	39.17	38.67	37.54	39.83	41.95	39.73	40.45	44.18	36.11	39.81	
		SSIM	0.9565	0.9853	0.9870	0.9849	0.9814	0.9777	0.9798	0.9875	0.9741	0.9822	
	Xformer	PSNR	39.06	38.66	38.04	40.07	41.93	39.72	40.46	44.11	36.17	39.89	
		SSIM	0.9560	0.9848	0.9877	0.9852	0.9792	0.9773	0.9794	0.9857	0.9743	0.9817	
KBNet	Restormer	PSNR	39.14	38.59	37.79	40.14	41.77	39.67	40.45	44.02	36.22	39.83	
		SSIM	0.9564	0.9843	0.9863	0.9855	0.9776	0.9773	0.9798	0.9850	0.9751	0.9814	
	NAFNet	PSNR	39.12	38.62	37.67	39.95	41.88	39.73	40.51	44.16	36.16	39.84	
		SSIM	0.9563	0.9849	0.9863	0.9853	0.9797	0.9776	0.9800	0.9861	0.9747	0.9818	
	KBNet	PSNR	39.13	38.62	37.61	39.89	41.76	39.80	40.57	44.22	36.07	39.82	
		SSIM	0.9564	0.9843	0.9861	0.9849	0.9761	0.9777	0.9798	0.9845	0.9743	0.9810	
	Xformer	PSNR	39.08	38.64	37.74	40.08	41.76	39.69	40.48	44.09	36.18	39.83	
		SSIM	0.9560	0.9845	0.9862	0.9851	0.9776	0.9772	0.9797	0.9849	0.9747	0.9812	
Xformer	Restormer	PSNR	39.09	38.60	37.81	40.25	42.12	39.72	40.51	44.10	36.28	39.92	
		SSIM	0.9558	0.9851	0.9859	0.9861	0.9831	0.9776	0.9801	0.9885	0.9753	0.9827	
	NAFNet	PSNR	39.17	38.62	37.73	40.18	42.29	39.75	40.56	44.27	36.19	39.95	
		SSIM	0.9563	0.9856	0.9860	0.9860	0.9851	0.9775	0.9806	0.9896	0.9750	0.9832	
	KBNet	PSNR	39.10	38.51	37.43	39.98	42.12	39.69	40.47	43.98	36.15	39.79	
		SSIM	0.9557	0.9851	0.9854	0.9852	0.9844	0.9774	0.9801	0.9889	0.9743	0.9826	
	Xformer	PSNR	39.10	38.75	37.82	40.29	42.20	39.89	40.70	44.44	36.25	40.04	
		SSIM	0.9557	0.9856	0.9862	0.9860	0.9826	0.9779	0.9807	0.9886	0.9751	0.9828	

Table 12. Quantitative comparisons of real-world denoising performance across various training set configurations. Methods marked with an asterisk (*) are evaluated using official out-of-the-box models.

Denoising network	Trained noise	Metric	SIDD	Poly	CC	HighISO	iPhone	Huawei	OPPO	Sony	Xiaomi	Total Avg.
Restormer [43]	SIDD*	PSNR	40.02	37.66	36.33	38.29	40.13	38.42	39.56	44.19	35.65	38.92
		SSIM	0.9603	0.9793	0.9807	0.9756	0.9734	0.9675	0.9773	0.9894	0.9710	0.9749
	SIDD + Gaussian	PSNR	39.67	37.61	35.52	38.08	40.38	38.51	39.83	43.72	35.54	38.76
		SSIM	0.9586	0.9800	0.9771	0.9765	0.9748	0.9690	0.9795	0.9865	0.9714	0.9748
	Ours	PSNR	39.22	38.76	37.68	40.14	41.85	39.72	40.64	44.29	36.19	39.83
		SSIM	0.9569	0.9854	0.9866	0.9857	0.9786	0.9766	0.9800	0.9871	0.9750	0.9791
NAFNet [6]	SIDD*	PSNR	39.97	37.17	35.69	38.32	40.25	37.73	39.64	43.65	34.99	38.60
		SSIM	0.9600	0.9717	0.9811	0.9788	0.9707	0.9680	0.9786	0.9829	0.9685	0.9734
	SIDD + Gaussian	PSNR	39.61	37.93	36.10	38.20	40.66	37.92	39.66	43.49	35.65	38.80
		SSIM	0.9582	0.9809	0.9797	0.9788	0.9779	0.9704	0.9815	0.9886	0.9716	0.9764
	Ours	PSNR	39.24	38.72	37.84	40.00	42.08	39.83	40.55	44.34	36.17	39.86
		SSIM	0.9570	0.9855	0.9877	0.9856	0.9812	0.9782	0.9801	0.9875	0.9749	0.9797

noising performance undergoes significant improvement. This enhancement can be attributed to our noise translation network, which effectively adapts the real-world noise into a form closer to the Gaussian noise that the pretrained model is adept at handling. Note that, in our pretraining approach, the denoising network is trained on Gaussian noise augmented with the same real-world noise used to train the noise translation network. This distinction in pretraining strategies explains the observed performance gap between the two results.

8.8. Effects of hyperparameters

Table 14 presents the ablative results of our hyperparameters, including pretraining noise level (σ), noise injection level ($\tilde{\sigma}$), explicit loss weight (α), and spatial frequency ratio (β). The pretraining level part of Table 14 shows the ablation results for the Gaussian noise levels added to create noisy input during denoising network pretraining. As the noise level increased, the performance on in-distribution (ID) consistently decreased. For out-of-distribution (OOD), the performance improved until noise level of 15, beyond

Table 13. Quantitative results of applying noise translation framework to denoising model pre-trained on pure synthetic Gaussian noise.

Denoising methods	Metric	SIDD	Poly	CC	HighISO	iPhone	Huawei	OPPO	Sony	Xiaomi	Total Avg.
Restormer-Gaussian [43]	PSNR	23.99	35.97	33.41	35.31	38.02	36.94	37.84	42.90	34.49	35.43
	SSIM	0.4990	0.9585	0.9563	0.9464	0.9448	0.9502	0.9629	0.9831	0.9554	0.9063
+ Ours	PSNR	39.08	37.88	35.75	39.33	41.21	38.44	39.96	43.18	35.63	38.94
	SSIM	0.9542	0.9832	0.9800	0.9827	0.9823	0.9719	0.9790	0.9835	0.9720	0.9765

Table 14. Sensitivity results on various hyperparameters in our framework.

Pretraining Level			Noise Injection Level			Explicit Loss Weight			Spatial-Frequency Ratio		
σ	SIDD	OOD Avg.	$\tilde{\sigma}$	SIDD	OOD Avg.	α	SIDD	OOD Avg.	β	SIDD	OOD Avg.
5	39.37	38.96	0	39.43	39.37	0	39.07	39.74	0	39.13	39.84
10	39.29	39.64	1	39.38	39.54	0.001	39.08	39.76	0.0005	39.16	39.88
15	39.24	39.94	5	39.09	39.78	0.005	39.11	39.80	0.001	39.18	39.91
20	38.88	39.53	15	39.15	39.86	0.01	39.14	39.85	0.002	39.24	39.94
25	38.73	39.21	50	39.15	39.90	0.05	39.24	39.94	0.005	39.17	39.94
			100	39.24	39.94	0.1	39.19	39.92	0.01	39.09	39.77
			200	39.19	39.93	0.5	39.13	39.07	0.02	39.00	38.97

which it began to degrade, due to oversmoothing effects caused by learning to handle strong noise. The noise injection level part presents the ablation results for Gaussian noise injection levels. Increasing the noise level led to a decline in ID performance, while OOD performance improved up to a certain point. The explicit loss weight and spatial-frequency ratio parts show the ablation results for the α and β values in Eq. (11) and (10), respectively. Overall, the ablation experiments determined the optimal hyperparameters as follows: a pretraining noise level $\sigma = 15$, a Gaussian noise injection level $\tilde{\sigma} = 100$, $\alpha = 5 \times 10^{-2}$, and $\beta = 2 \times 10^{-3}$.

8.9. Training Stability

To evaluate the stability of training our noise translation network, we conducted five independent training runs using different random seeds and measured the PSNR metrics across multiple datasets. The standard deviations for each dataset were as follows: SIDD (0.023), Poly (0.007), CC (0.021), HighISO (0.009), iPhone (0.008), Huawei (0.010), OPPO (0.016), Sony (0.022), and Xiaomi (0.020). The average standard deviation across all datasets was 0.013, confirming the robustness and stability of training with our framework.

9. Qualitative Analysis

9.1. Additional OOD datasets and SIDD dataset

Qualitative results on all datasets in the main paper are shown in Figures 9, 10, 11 and 12. Our method significantly surpasses the PSNR scores of other denoising models on all OOD datasets (iPhone, Huawei, OPPO, Sony, Xiaomi). For the in-distribution SIDD, our method produces clean results without generating unnecessary zipper artifacts.

9.2. NIND (Natural Image Noise Dataset)

The NIND [3] dataset comprises high-resolution images captured at various ISO levels. High ISO images are noisier due to increased sensor sensitivity, while low ISO images, though cleaner, may require more optimal settings or equipment to capture effectively. Figure 13 and Figure 14 illustrate the qualitative results of our method applied to high ISO images, demonstrating its ability to effectively remove noise while preserving fine image details. The denoised outputs are visually clean and free from artifacts, achieving a quality comparable to images captured at low ISO levels.

9.3. Real-world smartphone image noise and denoising results

Finally, we present the denoised results of images captured using our Galaxy S22+ smartphone, as shown in Figure 15.

10. Limitations

Although our approach provides strong robustness to diverse real-world noise, it may appear to compromise performance on in-distribution (ID) datasets. As discussed in Figure 8, this effect is largely due to the pronounced overfitting of conventional denoising models, which tend to reconstruct dataset-specific artifacts rather than genuine image content.

Moreover, our evaluation primarily relies on PSNR and SSIM computed against the provided ground-truth images. While these metrics are standard practice, they inherently struggle to capture perceptual realism and may not align well with human judgments. Although our method consistently improves these metrics, such quantitative measures do not fully represent perceptual quality, which remains subjective and can vary across viewers. Future work includes exploring alternative evaluation protocols or perceptually aligned metrics that better account for realism, semantic consistency, and human preference.

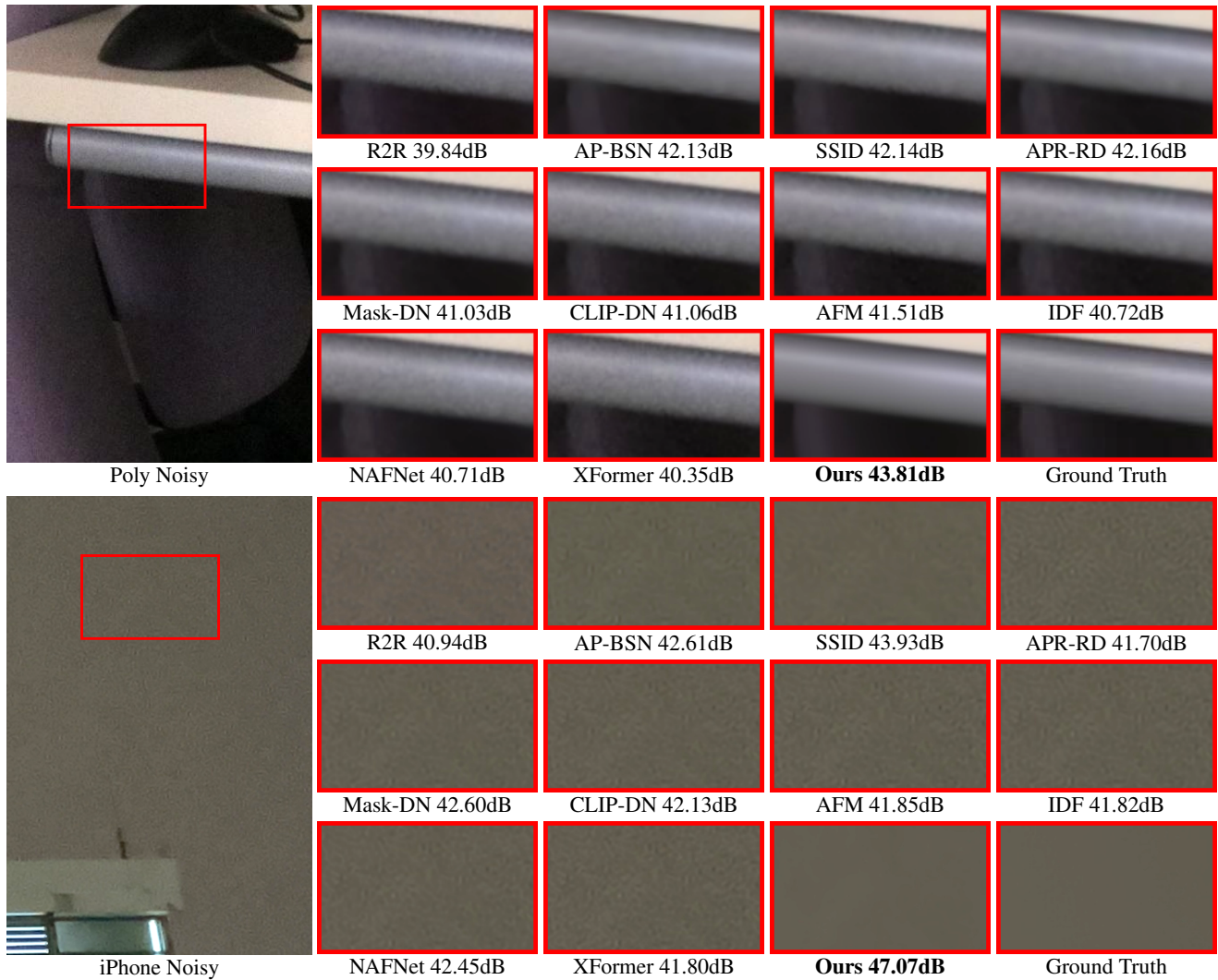


Figure 9. Comparison between the qualitative results of various denoising networks including ours (noise translation network with pre-trained NAFNet), on the out-of-distribution (OOD) datasets (Poly and iPhone). Our result displays cleaner outputs compared to other state-of-the-art networks that are directly trained from a real-noise dataset. Zoom in for better comparison.

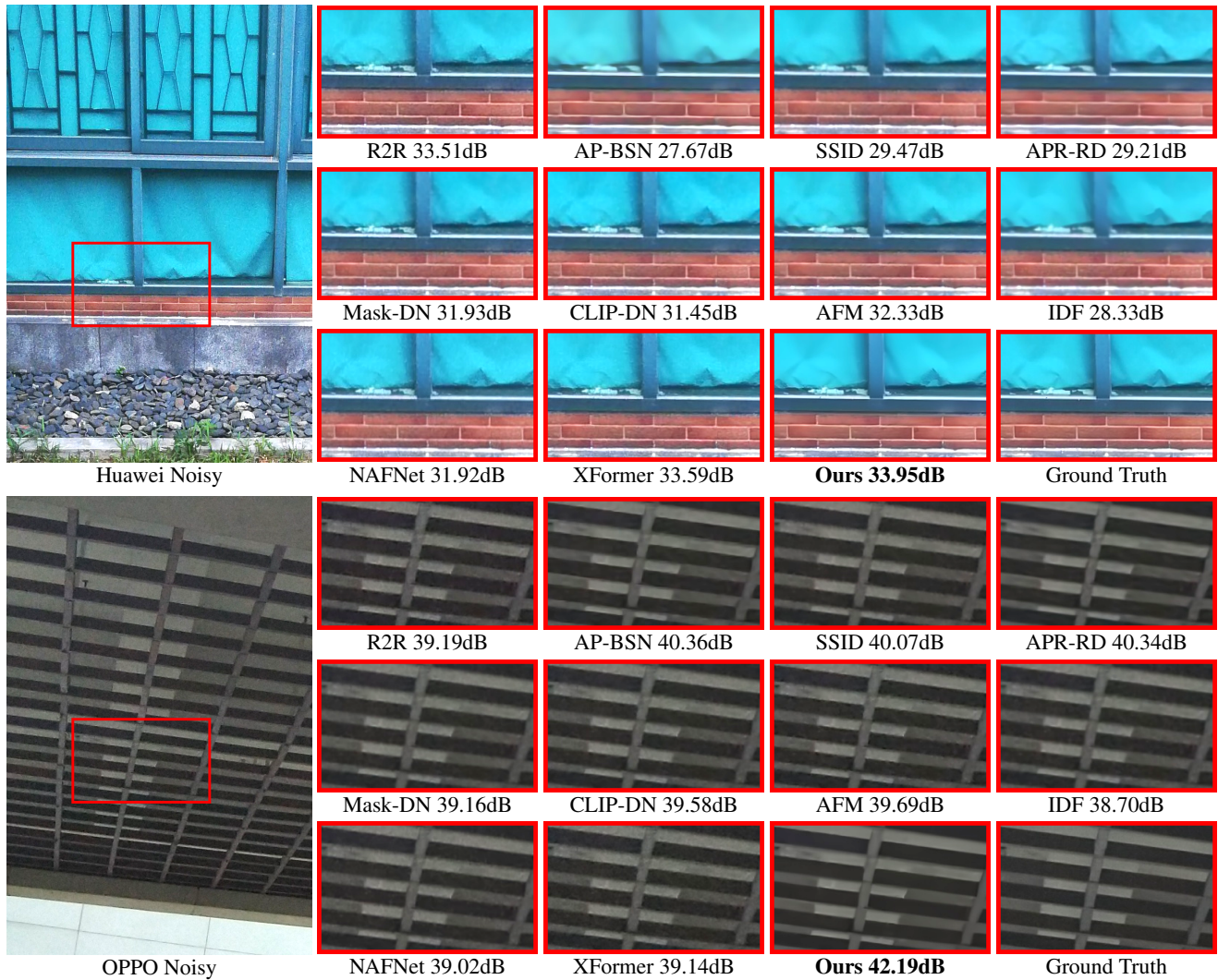


Figure 10. Comparison between the qualitative results of various denoising networks including ours (noise translation network with pretrained NAFNet), on the out-of-distribution (OOD) datasets (Huawei and OPPO). Our result displays cleaner outputs compared to other state-of-the-art networks that are directly trained from a real-noise dataset. Zoom in for better comparison.

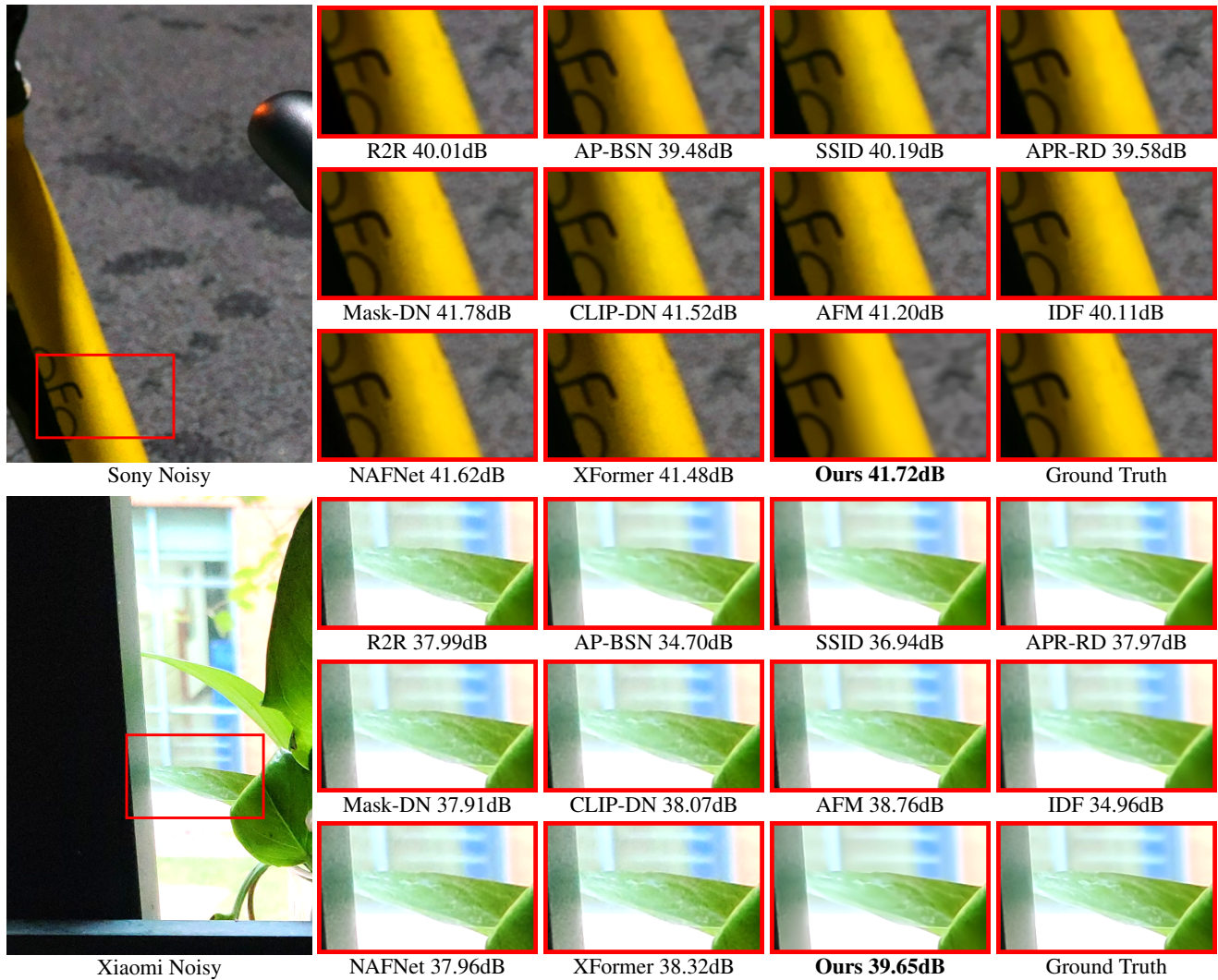


Figure 11. Comparison between the qualitative results of various denoising networks including ours (noise translation network with pretrained NAFNet), on the out-of-distribution (OOD) datasets (Sony and Xiaomi). Our result displays cleaner outputs compared to other state-of-the-art networks that are directly trained from a real-noise dataset. Zoom in for better comparison.

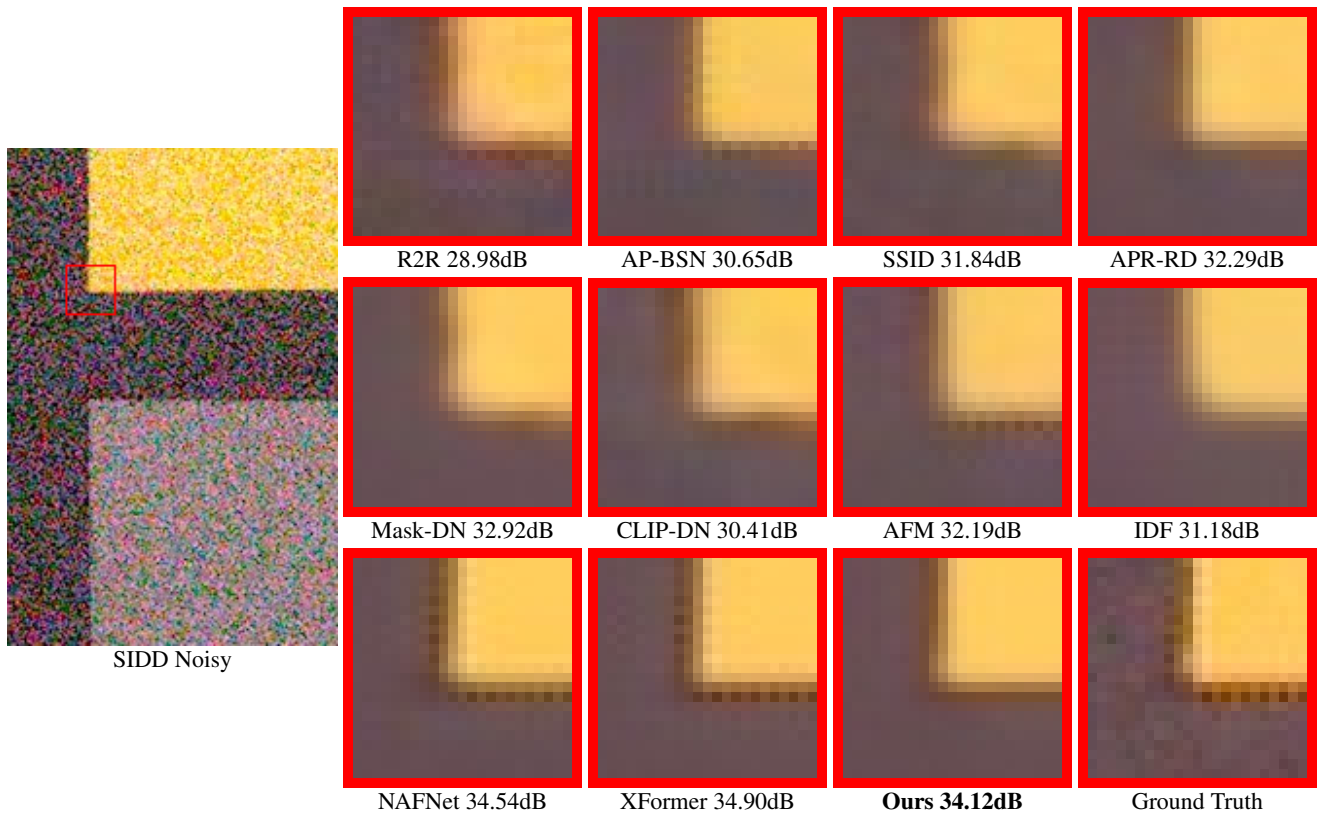


Figure 12. Comparison between the qualitative results of various denoising networks including ours (noise translation network with pretrained NAFNet), on the SIDD dataset. Our result displays competitive visual quality with real noise.

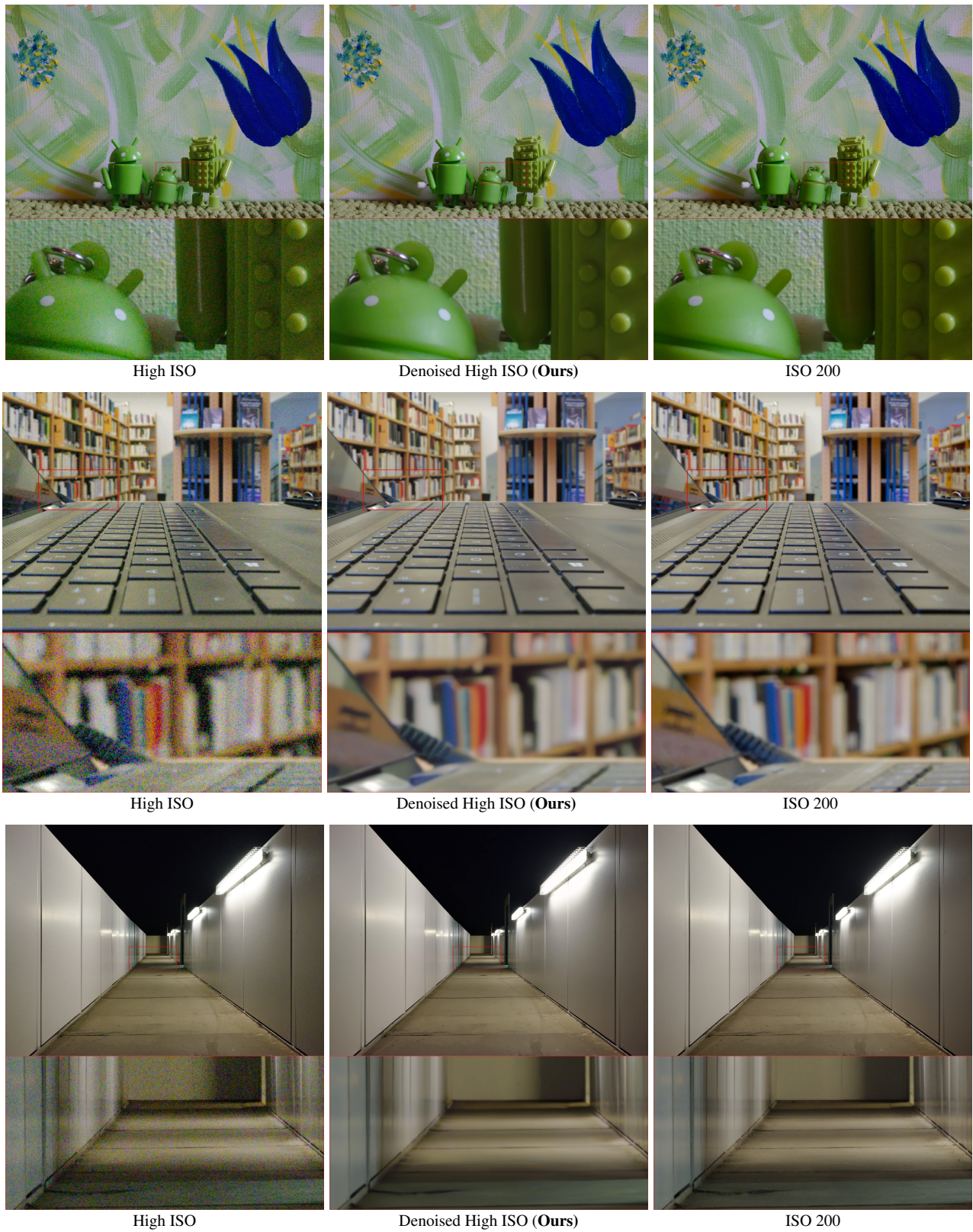


Figure 13. Qualitative results of our noise translation network with pretrained NAFNet applied to high ISO images from the NIND dataset. Our method effectively removes noise while preserving fine details, producing outputs comparable to low ISO (ISO 200) images. Zoom in for a closer inspection of the visual quality.

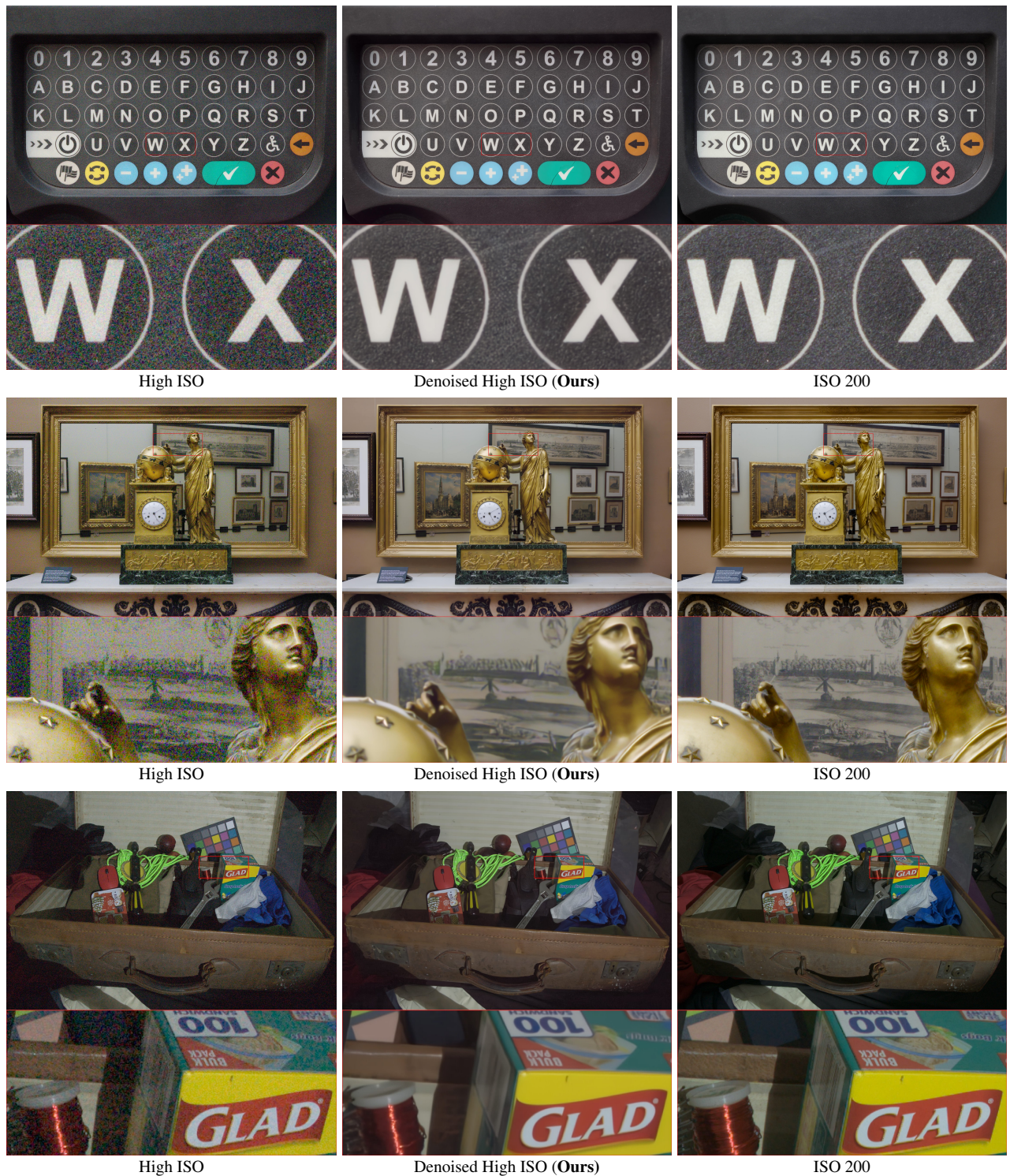


Figure 14. Qualitative results of our noise translation network with pretrained NAFNet applied to high ISO images from the NIND dataset. Our method effectively removes noise while preserving fine details, producing outputs comparable to low ISO (ISO 200) images. Zoom in for a closer inspection of the visual quality.

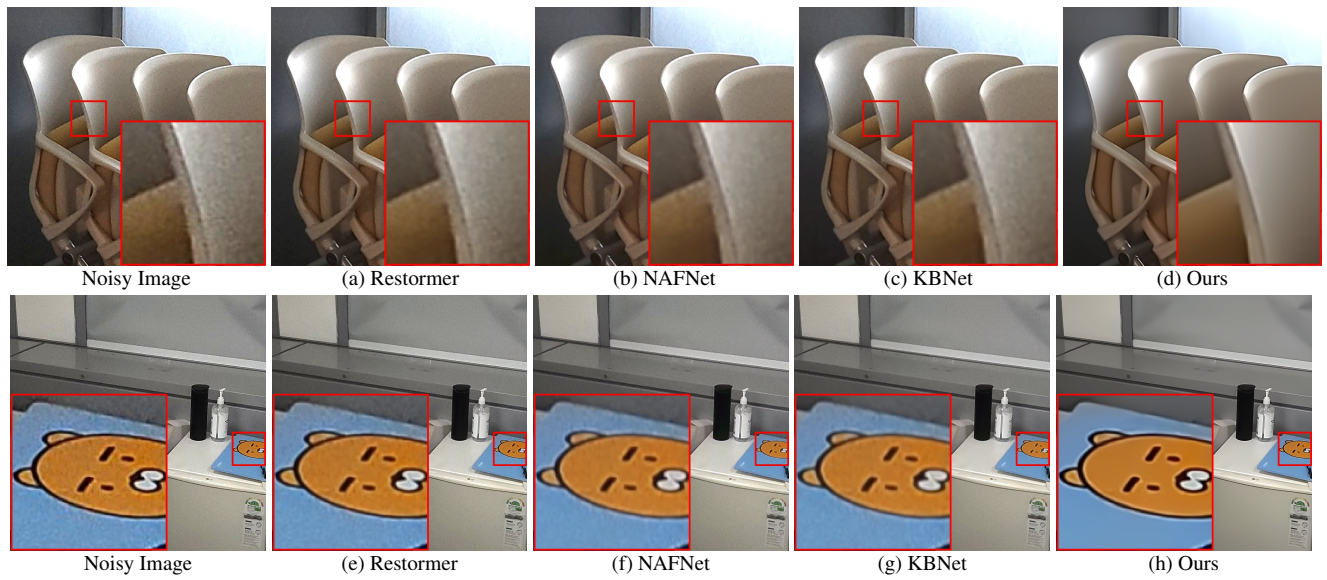


Figure 15. Comparison between the qualitative results of various denoising networks including ours (noise translation network with pretrained NAFNet) on images captured by Galaxy S22+ smartphone. Zoom in for a closer inspection of the visual quality.